

ORIGINAL RESEARCH

Exosomes From Induced Pluripotent Stem Cell–Derived Cardiomyocytes Promote Autophagy for Myocardial Repair

Michelle R. Santoso, BS, BA; Gentaro Ikeda, MD, PhD; Yuko Tada, MD, PhD; Ji-Hye Jung, PhD; Evgeniya Vaskova, PhD; Raymond G. Sierra, PhD; Cornelius Gati, PhD; Andrew B. Goldstone, MD, PhD; Daniel von Bornstaedt, MD; Praveen Shukla, MS, PhD; Joseph C. Wu, MD, PhD; Soichi Wakatsuki, PhD; Y. Joseph Woo, MD; Phillip C. Yang , MD

BACKGROUND: Induced pluripotent stem cells and their differentiated cardiomyocytes (iCMs) have tremendous potential as patient-specific therapy for ischemic cardiomyopathy following myocardial infarctions, but difficulties in viable transplantation limit clinical translation. Exosomes secreted from iCMs (iCM-Ex) can be robustly collected in vitro and injected in lieu of live iCMs as a cell-free therapy for myocardial infarction.

METHODS AND RESULTS: iCM-Ex were precipitated from iCM supernatant and characterized by protein marker expression, nanoparticle tracking analysis, and functionalized nanogold transmission electron microscopy. iCM-Ex were then used in in vitro and in vivo models of ischemic injuries. Cardiac function in vivo was evaluated by left ventricular ejection fraction and myocardial viability measurements by magnetic resonance imaging. Cardioprotective mechanisms were studied by JC-1 (tetraethylbenzimidazolylcarbocyanine iodide) assay, immunohistochemistry, quantitative real-time polymerase chain reaction, transmission electron microscopy, and immunoblotting. iCM-Ex measured \approx 140 nm and expressed CD63 and CD9. iCM and iCM-Ex microRNA profiles had significant overlap, indicating that exosomal content was reflective of the parent cell. Mice treated with iCM-Ex demonstrated significant cardiac improvement post–myocardial infarction, with significantly reduced apoptosis and fibrosis. In vitro iCM apoptosis was significantly reduced by hypoxia and exosome biogenesis inhibition and restored by treatment with iCM-Ex or rapamycin. Autophagosome production and autophagy flux was upregulated in iCM-Ex groups in vivo and in vitro.

CONCLUSIONS: iCM-Ex improve post–myocardial infarction cardiac function by regulating autophagy in hypoxic cardiomyocytes, enabling a cell-free, patient-specific therapy for ischemic cardiomyopathy.

Key Words: autophagy ■ exosomes ■ iPSC ■ ischemic cardiomyopathy

The development of patient-specific induced pluripotent stem cells (iPSCs) has unprecedented therapeutic potential for the treatment of cardiac ischemia arising from myocardial infarction (MI). iPSCs can be readily differentiated into contractile cardiomyocytes (iCMs) and transplanted into the myocardium.^{1,2} Despite initial enthusiasm, the lack of sustained cell engraftments has restricted clinical translation.^{3,4} Intriguingly, even in cases of minimal

iCM engraftment, we and other groups have reported significant improvement in cardiac function and attribute much of the putative effect to paracrine factors.^{5–7}

Exosomes are a subset of extracellular vesicles and are important messengers of paracrine activity. They are typically 30 to 150 nm in diameter⁸ and are found abundantly in the secretome of many cell types, including cardiac progenitor cells,⁹ embryonic stem cells,¹⁰ and iPSCs.¹¹ Exosomes carry various bioactive

Correspondence to: Phillip C. Yang, MD, 269 Campus Drive, CCSR 3115, Stanford, CA 94305. E-mail: phillip@stanford.edu

Supplementary material for this article is available at <https://www.ahajournals.org/doi/suppl/10.1161/JAHA.119.014345>

For Sources of Funding and Disclosures, see page 13.

© 2020 The Authors. Published on behalf of the American Heart Association, Inc., by Wiley. This is an open access article under the terms of the Creative Commons Attribution-NonCommercial-NoDerivs License, which permits use and distribution in any medium, provided the original work is properly cited, the use is non-commercial and no modifications or adaptations are made.

JAHA is available at: www.ahajournals.org/journal/jaha

CLINICAL PERSPECTIVE

What Is New?

- Induced pluripotent stem cell–derived cardiomyocytes (iCM) and iCM-derived exosomes provide comparable therapeutic benefit in murine and in vitro models of cardiac ischemia.
- iCM-derived exosome treatment reduces apoptosis and fibrosis post–myocardial infarction.
- iCM-derived exosomes promote autophagy and autophagic flux in hypoxic cardiomyocytes and in the peri-infarct region.

What Are the Clinical Implications?

- iCM-derived exosomes are a potential cell-free, nontumorigenic therapy to facilitate clinical translation of induced pluripotent stem-cell technology.

Nonstandard Abbreviations and Acronyms

iCM	iPSC-derived iCM
iCM-Ex	iCM-derived exosomes
iPSC	induced pluripotent stem cell
LVEF	left ventricular ejection fraction
MEMRI	manganese-enhanced MRI
MI	myocardial infarction
MMP	mitochondrial membrane potential
NTA	nanoparticle tracking analysis
PIR	peri-infarct region
TEM	transmission electron microscopy

molecules, such as microRNAs (miRNAs) and proteins, that reflect their cell of origin¹² and functionally alter recipient cells. We previously reported the cardioprotective benefits of iCM transplantation⁷ and thus sought to determine if iCM-derived exosomes may similarly have therapeutic potential.

Autophagy is a conserved metabolic process that involves the engulfment of cytoplasmic material into membrane-bound vesicles called autophagosomes and the fusion and subsequent degradation of autophagosomes with lysosomes, releasing molecular building blocks and energy.¹³ Autophagy occurs constitutively on a basal level, but it is further activated during stress and starvation.¹⁴ Regulation of autophagosome turnover, hereafter referred to as autophagic flux, is essential to maintain cellular health. Impairment of autophagic flux has been linked to neurological, renal, inflammatory, and cardiovascular diseases.¹⁴

Groups have reported that various adult stem cell–derived exosomes may mediate autophagic signaling in recipient cells.¹⁵ It remains unknown, however, if iPSC and iPSC-differentiated cells produce exosomes that regulate autophagy.

In this article we show that iCM-derived exosomes (iCM-Ex) largely mimic iCMs and preserve cardiac function, myocyte viability, and exert antiapoptotic signaling in MI models. We provide evidence that iCM-Ex modulates signaling pathways upstream of autophagy and upregulates autophagy to maintain cardiac homeostasis. Finally, we demonstrate that autophagic flux, which is impaired in ischemic conditions, is restored by iCM-Ex.

METHODS

Detailed methods can be found in Data S1.

In accordance with the Transparency and Openness Promotion Guidelines, the data that support the findings of this study are available from the corresponding author on request. This study has been approved by Stanford University School of Medicine Institutional Review Board committee and Institutional Animal Care and Use Committee (IRB Approval Number 17775, 31689; IACUC Assurance Number A3213-01).

iCM-Ex Isolation

Exosomes were isolated from cell culture supernatant by polyethylene glycol precipitation as described by other groups.^{16,17} iCM supernatant was collected, centrifuged at 1500g for 10 minutes, passed through a 0.22- μ m filter to remove cell debris, then incubated overnight with polyethylene glycol 8000 (Millipore Sigma, St. Louis, MO) at 4°C. The solution containing exosomes was then centrifuged at 1500g for 30 minutes and 300g for 5 minutes to form a pellet. The supernatant was removed, and the pellet was resuspended in sterile PBS.

In Vitro Hypoxia Model

Cell media were changed to glucose- and supplement-depleted media and placed in a Hypoxia Inductor Chamber (Stemcell Technologies, Vancouver, BC, Canada). The oxygen content was reduced to 0% or 1% using a N₂/CO₂ gas mix. The chamber was subsequently placed in a 37°C incubator.

Murine Acute MI Model

Animal care and interventions were done in accordance with the Laboratory Animal Welfare Act and Stanford University Administrative Panel on Laboratory Animal Care. All animals received humane care and treatment in accordance with the

Guide for the Care and Use of Laboratory Animals (www.nap.edu/catalog/5140.html). Female severe combined immunodeficient beige mice were purchased from Charles River (Wilmington, MA). The mice selected for surgeries were 60 to 100 days old, nonpregnant, and demonstrating normal grooming and ambulatory behavior. Experimental groups were randomized across multiple cages, litters, and location of mouse cages in the husbandry room. An unblinded researcher labeled control/treatment injections in an Eppendorf tube labeled with random numbers. Surgeons were blinded and labeled mice by injections using ear and/or tail cuts. Mice sustained MIs as previously described.⁷ A blinded surgeon injected 60 μ L of iCM-Ex (4×10^8) or iCMs (500 000) suspended in a 1:1 mixture of PBS and Matrigel (Corning Life Sciences, Tewksbury, MA) at the peri-infarct region (PIR): iCMs (n=6), iCM-Ex (n=8), saline control (n=12). Matrigel was used to improve engraftment in the myocardium. Post-MI magnetic resonance images (MRI) were collected and analyzed blindly. Mice with ejection fraction >45% as measured by cardiac MRI were excluded from the final analysis. The final allocation of mice across control/experimental groups was concealed from the surgeon(s) and MRI operators.

Statistical Analyses

Data are presented as mean \pm SEM. Statistical significance was determined by Student t test for comparisons of 2 groups or by 1-way ANOVA followed by a post hoc Tukey test for comparisons among 3 or more groups (Prism 8, GraphPad Software, San Diego, CA). For arrays, statistical analysis was performed using Affymetrix Expression Console and Transcriptome Analysis Console software and Ingenuity Pathway Analysis (Qiagen, Hilden, Germany).

RESULTS

Characterization of iCMs and iCM-Ex

Whole-cell patch clamp was used to assess iCM electrophysiological properties to determine specific cell types. Action potentials, iCM subtypes, and their respective patch clamp measurements of action potential durations and their specific characteristics confirm the cardiac phenotypes of the iCMs (Figure 1A through 1D; Tables S1, S2). Extracellular vesicles from iCM-conditioned media were precipitated then probed for expression of the canonical exosomal marker CD63 (Figure 1E; Table S3A-B). Nanoparticle tracking analysis of the precipitate revealed a homogeneous population of vesicles of diameter 80 to 200 nm with a mode at 142 nm (Figure 1F). Signals

greater than 142 nm appeared to be multiples of 142 (eg, 295 $\approx 142 \times 2$), suggesting particle aggregates. These data indicated that extracellular vesicles were largely exosomes (iCM-Ex) and not microvesicles or apoptotic bodies, which have been characterized as larger than exosomes. Finally, we imaged iCM-Ex by immunogold transmission electron microscopy. The iCM-Ex were incubated with an antibody for exosomal marker CD9, then conjugated to functionalized nanogold (Table S3C-D). CD9-nanogold complexes were detected in iCM-Ex samples as imaged by transmission electron microscopy, appearing as hyperintense dots (Figure 1G).

iCM-Ex Promote Survival of Hypoxic Cardiomyocytes

We previously demonstrated that iCM transplantation enhances cardiomyocyte survival in ischemia largely through secretion of cardioprotective paracrine factors.⁷ Exosomes may be a vehicle for stem cell paracrine factors, and their molecular contents may mirror the parent cell. miRNA profiling of iCMs and iCM-Ex revealed that the majority (97.4%) of miRNAs in iCM-Ex were expressed at similar levels in iCMs (less than 2-fold change) (Figure S1A through S1C). miRNA expression within groups was normalized to housekeeping miRNAs.

We next determined if iCM-Ex may confer cardioprotection in ischemic conditions. iCM-Ex were transfected with fluorescent short interfering RNA and incubated with hypoxic iCM-Ex. One hour later, hypoxic iCMs stained with cardiomyocyte troponin marker *TNNI3* showed positive colocalized short interfering RNA fluorescence, indicating successful uptake of iCM-Ex in hypoxic conditions (Figure 2A; Table S4E-F). We also treated hypoxic iCMs with manumycin A (MA), a suppressor of exosome biogenesis through nSMase2 (neutral sphingomyelinase 2) inhibition. nSMase2 regulates exosome secretion by triggering the budding of exosomes into multivesicular bodies.¹⁸ Pharmacological inhibitors of nSMase2 (eg, MA) have been used to suppress exosome secretion.^{19,20} An MA dose concurrent with work by Mittelbrunn and colleagues (10 μ mol/L)²¹ successfully suppressed exosome biogenesis quantified by acetylcholinesterase activity (Figure 2B). iCMs were then exposed to acute hypoxia (8 hours, 0.1% to 0.3% O₂) and treated with iCM-Ex, MA, or neither and evaluated for early apoptosis by JC-1 assay, which measures mitochondrial membrane potential (Figure 2C and 2D).²² Hypoxia significantly reduced mitochondrial membrane potential (normoxia 1.00 ± 0.13 versus hypoxia (-) 0.46 ± 0.06 , $P < 0.01$), signifying early apoptosis. Treatment with autologous iCM-Ex abrogated this effect and significantly restored mitochondrial membrane potential

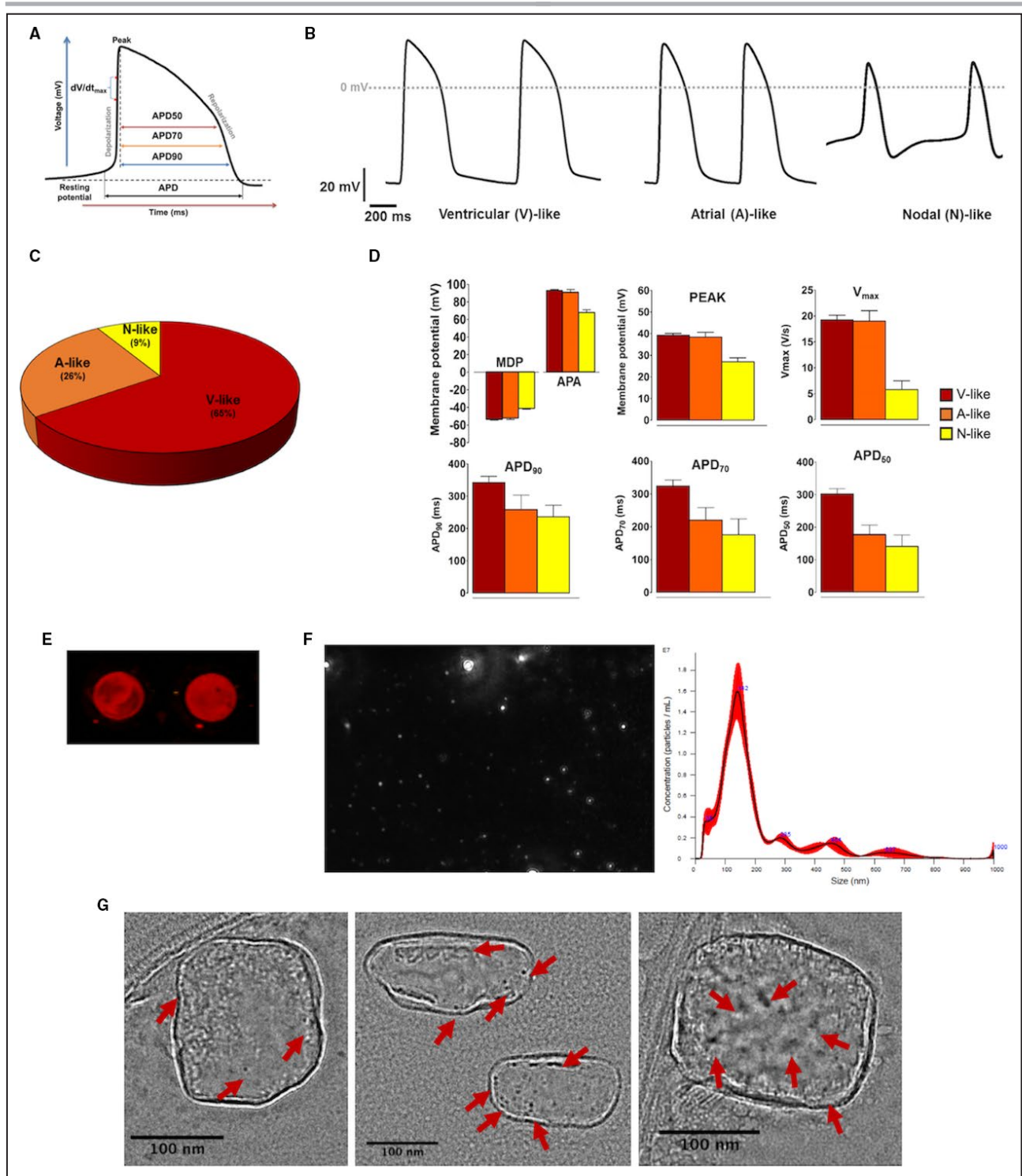


Figure 1. Characterization of iCMs and iCM-Ex.

A, Schematic diagram of an action potential (AP) trace of iCMs, showing how results were analyzed to calculate AP duration at 50%, 70%, and 90% repolarization (APD₅₀, APD₇₀, and APD₉₀, respectively). **B**, Representative AP recordings using whole-cell patch clamp of iPSC-derived cardiomyocytes (iCMs). Cells exhibited AP morphologies that can be categorized as ventricular (V)-, atrial (A)-, or nodal (N)-like CMs. **C**, Subtype distribution of iCMs (n=23). **D**, Patch-clamp recordings of iCMs demonstrating maximal diastolic potential (MDP), action potential amplitude (APA), overshoot/peak voltage, V_{max} (maximal rate of depolarization), APD₅₀, APD₇₀, and APD₉₀. **E**, iCM-conditioned medium was precipitated and immunoblotted for CD63 (red). **F**, Nanoparticle tracking analysis (NTA) measured sizes and concentration of EVs in the precipitate of iCM-conditioned medium. **G**, TEM images of CD9-nanogold iCM-Ex. CD9 bonded to the antibody-gold complexes appears as hyperintense dots (indicated by red arrows). CM indicates cardiomyocyte; EV, extracellular vesicles; iCM, induced CM; iCM-Ex, exosomes secreted by iCM; iPSC, induced pluripotent stem cell; and TEM, transmission electron microscopy.

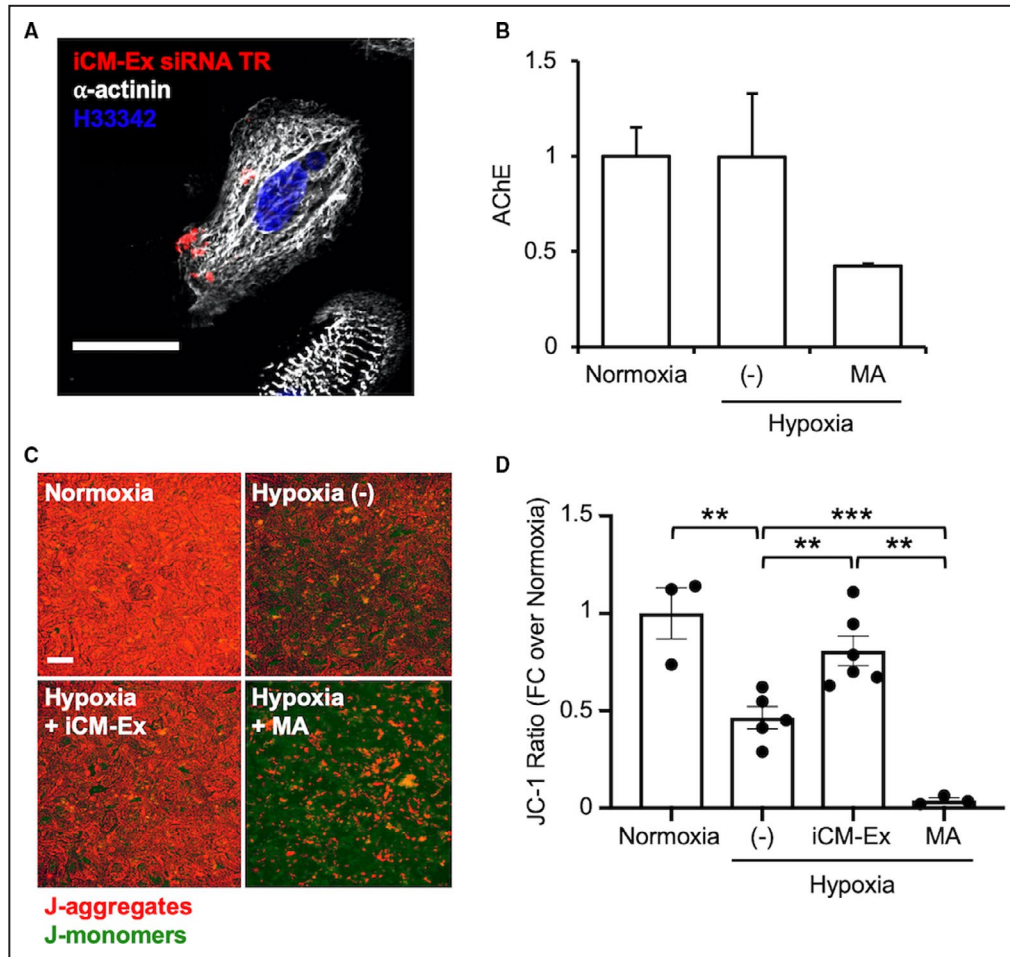


Figure 2. iCM-Ex are internalized and improve viability in iCMs after hypoxia.

A, iCM-Ex labeled with fluorescent siRNA are internalized into hypoxic iCMs. Scale bar=50 μ m. **(C)** Supernatants from 3 groups of iCMs were compared: normoxic, hypoxic untreated (-) control, and hypoxic + 10 μ mol/L manumycin A (MA). Exosome quantity in the supernatant was measured by acetylcholinesterase (AChE) activity. **(C)** Mitochondrial membrane potential (MMP) was assessed by JC-1 fluorescent assay of 4 groups: normoxia, hypoxia untreated (-) control, hypoxia + iCM-Ex, and hypoxia + 10 μ mol/L MA. Scale bar=100 μ m. **(D)** MMP is significantly reduced in hypoxic (-) or MA-treated cells and restored by iCM-Ex. ** P <0.01, *** P <0.001. FC indicates fold change; iCM, induced cardiomyocyte; iCM-Ex, exosomes secreted by iCM; siRNA, small interfering RNA; and (-), untreated control.

(hypoxia (-) versus hypoxia iCM-Ex 0.81 ± 0.08 , P <0.05). Additionally, MA exacerbated early apoptosis (hypoxia (-) versus hypoxia MA 0.04 ± 0.01 , P <0.05), suggesting that suppression of endogenous exosomes worsens apoptosis. Taken together, these findings suggest that exosomes confer endogenous protection from apoptosis, and exogenous provision of iCM-Ex may be cardioprotective.

iCM or iCM-Ex Improve Cardiac Function and Cell Survival in Murine MI Model

We next evaluated whether iCM-Ex could provide cardioprotection in a murine MI model. Prior work by Wang et al²³ suggested an effective dose of 2 μ g/g (as determined by protein quantitation assays) of

mesenchymal stem cell-derived exosomes. We performed Bradford and nanoparticle tracking analyses and determined that 0.05 μ g exosomes (for a 25-mg mouse) equated to roughly 4×10^8 particles and subsequently used this dose. To determine if Matrigel could enhance retention of injected nanoparticles, we compared injections of ferumoxytol in a mixture of Matrigel/PBS against ferumoxytol in PBS alone. Ferumoxytol nanoparticles in the mouse myocardium were detected as hypointense signals in cardiac MRI. Compared with the PBS group, ferumoxytol injected with Matrigel/PBS was retained longer, in greater volumes, and as a greater percentage of left ventricular (LV) area (Figure S2). We therefore used a Matrigel/PBS mixture to inject iCM, iCM-Ex, and the saline control.

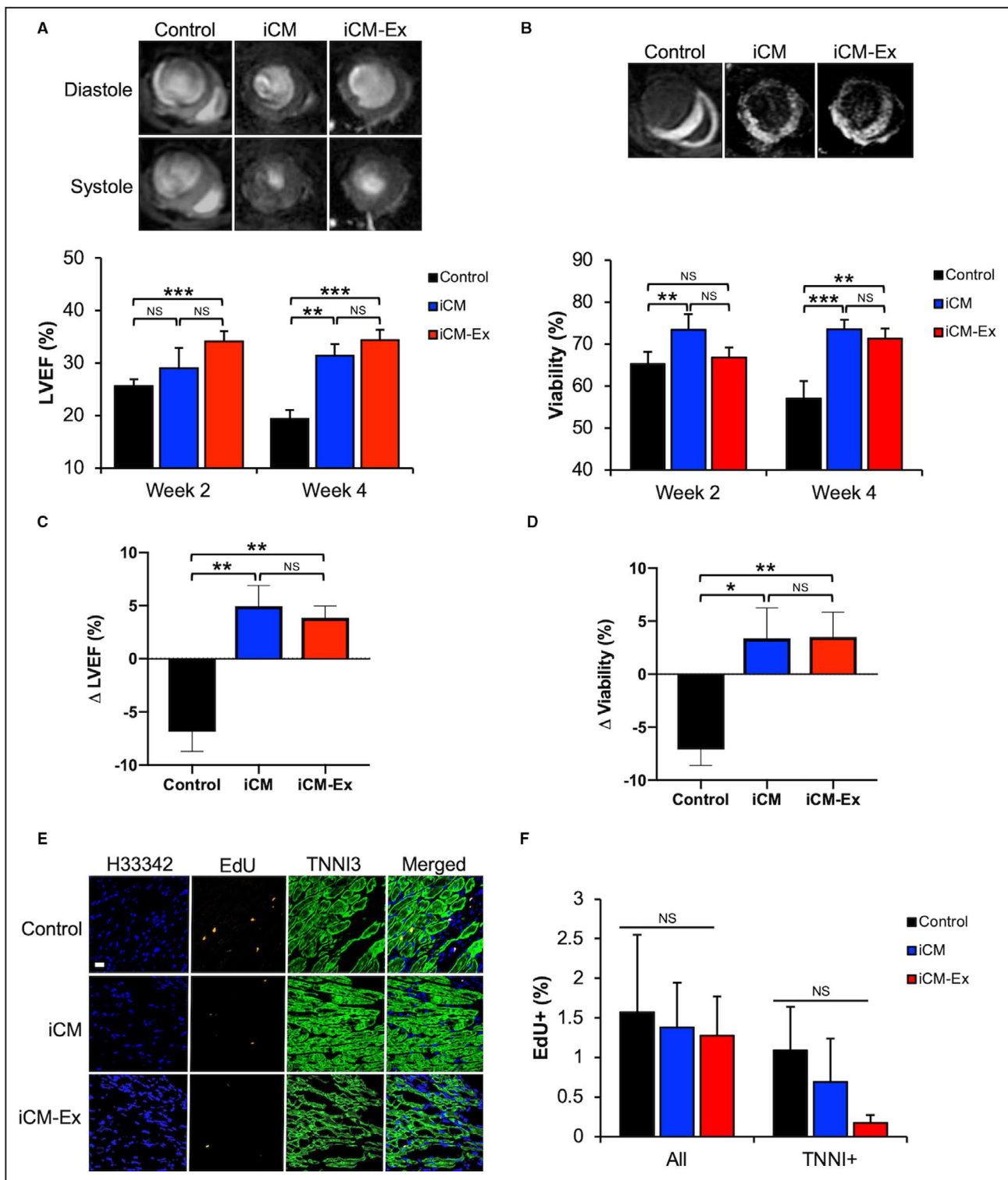


Figure 3. iCM-Ex improve cardiac function post-MI in vivo.

A, LV end-diastole and end-systole MR images of mice treated with saline control, iCMs, or iCM-Ex. LVEF measurements of saline control, iCM, and iCM-Ex mice at weeks 2 and 4 post-MI. **B**, Manganese-enhanced MR images. Hypointensity denotes viable myocardium. Quantitation of myocardial viability weeks 2 and 4 post-MI. **C**, Percentage differences in LVEF between week 2 and week 4. **D**, Percentage differences in myocardial viability between week 2 and week 4. **E**, LV sections from saline control, iCM, and iCM-Ex mice stained with EdU (red) and TNNI3 (green) antibodies and Hoechst 33 342 (blue). Scale bar=20 μ m. **F**, Percentage of EdU-positive cells and EdU/TNNI3 double-positive cells in the PIR. Data are mean \pm SEM of minimum n=3. * P <0.05, ** P <0.01, *** P <0.001. iCM indicates induced cardiomyocyte; iCM-Ex, exosomes secreted by iCM; LV, left ventricular; LVEF, LV ejection fraction; MR, magnetic resonance; NS, not statistically significant; and PIR, peri-infarct region.

Severe combined immunodeficient mice were subjected to acute MI and received intramyocardial injections of iCM (n=6), iCM-Ex (n=8), or saline control (n=12). Cardiac MRI demonstrated preserved systolic function in iCM and iCM-Ex mice compared with the control (Figure 3A). LV ejection fraction was significantly improved in iCM-Ex mice at week 2 (control 24.8±1.6% versus iCM-Ex 34.4±2.2%, $P<0.001$) and week 4 (control 19.7±5.2% versus iCM-Ex 35.7±1.7%, $P<0.001$) post-MI and in iCM-treated mice at week 4 (control versus iCM 31.4±2.2%, $P<0.01$). Myocardial viability, quantified by manganese-enhanced MRI, was greater in iCM mice at week 2 (control 58.9±2.9% versus iCM 73.4±3.7%, $P<0.01$) and at week 4 (control 46.0±2.4% versus iCM-Ex 71.7±3.2%, $P<0.01$) (Figure 3B). Longitudinal comparisons of LV ejection fraction demonstrated statistically significant differences between the week-2 to week-4 LV ejection fraction in control and iCM mice (control -6.9±1.9% versus iCM 5.0±2.0%, $P<0.01$) and control and iCM-Ex mice (control versus iCM-Ex +3.9±1.1%, $P<0.01$), but not between iCM and iCM-Ex mice (Figure 3C). Myocardial viability between weeks 2 and 4 demonstrated a similar pattern, deteriorating in control mice but sustained following iCM treatment (control -7.1±1.5% versus iCM 3.4±2.9%, $P<0.01$) or iCM-Ex treatment (control versus iCM-Ex 3.5±2.3%, $P<0.05$). Percentage differences in viability of iCM and iCM-Ex mice were statistically insignificant (Figure 3D). Together, these results indicate that iCM and iCM-Ex comparably preserve cardiac function and viability.

Increases in myocardial viability might be explained by endogenously proliferating stem cells in the mouse myocardium. To test this, mice were injected with 5-ethynyl-2'-deoxyuridine (EdU), a synthetic labeled nucleoside to label sites of DNA synthesis. Immunohistochemistry revealed no observable differences in the incorporation of the labeled nucleoside in *TNNI3*-stained cardiomyocytes of control, iCM, or iCM-Ex mice, indicating no differences in proliferation (Figure 3E and 3F; Table S3F-G). These data suggest that differences in myocardial viability are not attributed to active regeneration of the mouse myocardium but may instead be explained by salvage of the existing but injured cells.

Trichrome staining of LV cross sections at week 4 post-MI revealed significantly reduced fibrotic tissue in iCM and iCM-Ex mice (control 40.8±0.6% versus iCM 3.3±1.5%, $P<0.001$; control 40.8±0.6% versus iCM-Ex 13.4±2.5%, $P<0.01$) (Figure 4A and 4B). To test whether cardiomyocyte apoptosis is affected by iCM-Ex, we stained LV tissue for double-stranded DNA breaks (terminal deoxynucleotidyl transferase dUTP nick end labeling) and cardiac troponin I (*TNNI3*) (Figure 4C). There were significantly fewer terminal

deoxynucleotidyl transferase dUTP nick end labeling-positive cardiomyocytes in iCM- or iCM-Ex-treated hearts (control 33.1±3.0% versus iCM 6.6±6.6%, $P<0.001$; control 33.1±3.0% versus iCM-Ex 9.5±5.1%, $P<0.01$) (Figure 4D; Table S3F-G). To venture into the mechanism in which iCM-Ex confers antiapoptotic effects, we speculated whether the Bcl-2 family proteins might be involved. Quantitative real-time polymerase chain reaction of the tissues from the PIR demonstrated a trend of upregulation of prosurvival *BCL-X_L* and *BCL-2* in the iCM and iCM-Ex mice (Figure 4E and 4F; Table S4A-C). To study this finding, we sought to investigate the prosurvival mechanism caused by exosomes.

Pathway Regulation by iCM-Ex Treatment in Murine Myocardial Injury Model

A key function of exosomes is to influence gene expression and physiological pathways in recipient cells. We conducted transcriptomic analyses of the PIR of iCM, iCM-Ex, and control groups. Hierarchical clustering of gene expression demonstrated that iCM and iCM-Ex groups exhibited more similar expression patterns with each other compared with controls, again suggesting that iCM and iCM-Ex may be therapeutically interchangeable (Figure 5A).

A total of 1901 genes exhibited biologically significant differential expression ($P<0.05$, fold change $>|2|$) in treated versus untreated groups (886 genes were upregulated, 1015 genes were downregulated) (Figure 5B). We conducted pathway analyses to predict the physiological consequences and narrow down possible targets of these differentially expressed genes. The most enriched pathways included PI3K-Akt-mTOR, insulin, and MAPK signaling pathways (Figure 5C). Ingenuity pathway analysis predicted overall inhibition of the mammalian target of rapamycin (mTOR) signaling pathway (Figure 5D). We validated expression of several genes through quantitative real-time polymerase chain reaction (mTOR, control 1.00±0.13 versus iCM-Ex 0.42±0.05, $P<0.05$) (FKBP1, control 1.00±0.04 versus iCM-Ex 2.31±0.37, $P<0.05$) (Figure 5D; Table S4C-G). Together, these findings suggest that the inhibition of mTOR signaling in iCM-Ex groups may explain the observed physiological effects.

iCM-Ex Increases Autophagy and Autophagic Flux in Hypoxic iCMs

Because mTOR inhibition and the Bcl-2 family are known regulators of autophagy, we hypothesized that autophagy may be modulated by iCM-Ex. The transcriptome of iCM-Ex mice revealed enrichment of other signaling pathways that mediate autophagy (insulin and MAPK signaling pathways) (Figure 5C). Additionally, we found that induction of autophagy by rapamycin significantly preserves mitochondrial

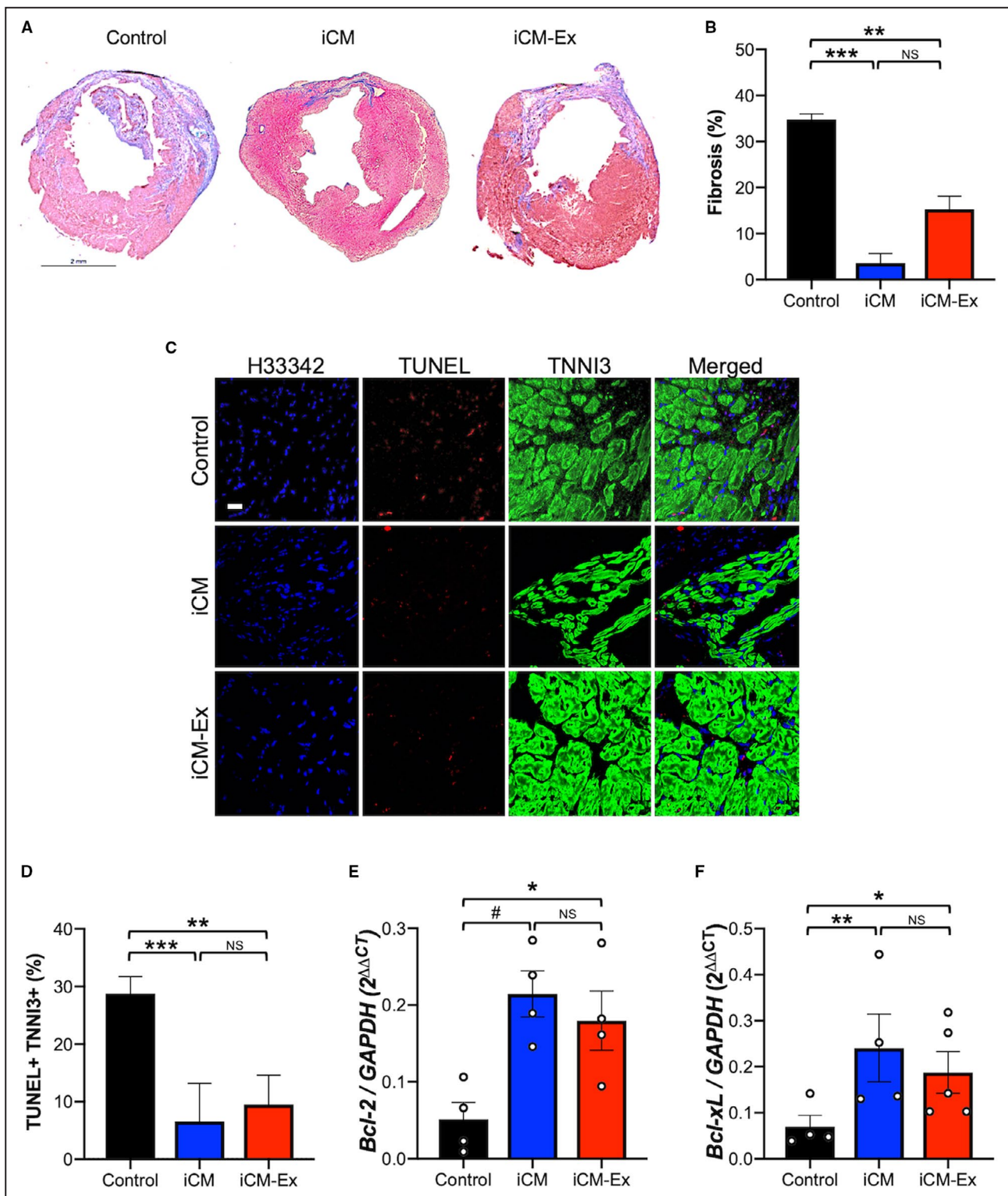


Figure 4. iCM-Ex improve cardiac cell survival.

A, Masson trichrome–stained mid-LV sections of saline control, iCM, and iCM-Ex mice. **B**, Percentage of fibrotic area in LV. **C**, LV sections from saline control, iCM, and iCM-Ex mice were costained with TUNEL (red) and TNNI3 (green) antibodies and Hoechst 33 342 (blue). Scale bar=20 μ m. **D**, Percentage of apoptotic cardiomyocytes. **E**, PIR of saline control, iCM, and iCM-Ex mice was isolated for qRT-PCR of **(E)** *Bcl-2* and **(F)** *Bcl-xL* expression, normalized to GAPDH. Data are mean \pm SEM of minimum n=3. * P <0.05, ** P <0.01, *** P <0.001. iCM indicates induced cardiomyocyte; iCM-Ex, exosomes secreted by iCM; LV, left ventricular; NS, not statistically significant; PIR, peri-infarct region; qRT-PCR, quantitative real-time polymerase chain reaction; and TUNEL, terminal deoxynucleotidyl transferase dUTP nick end labeling.

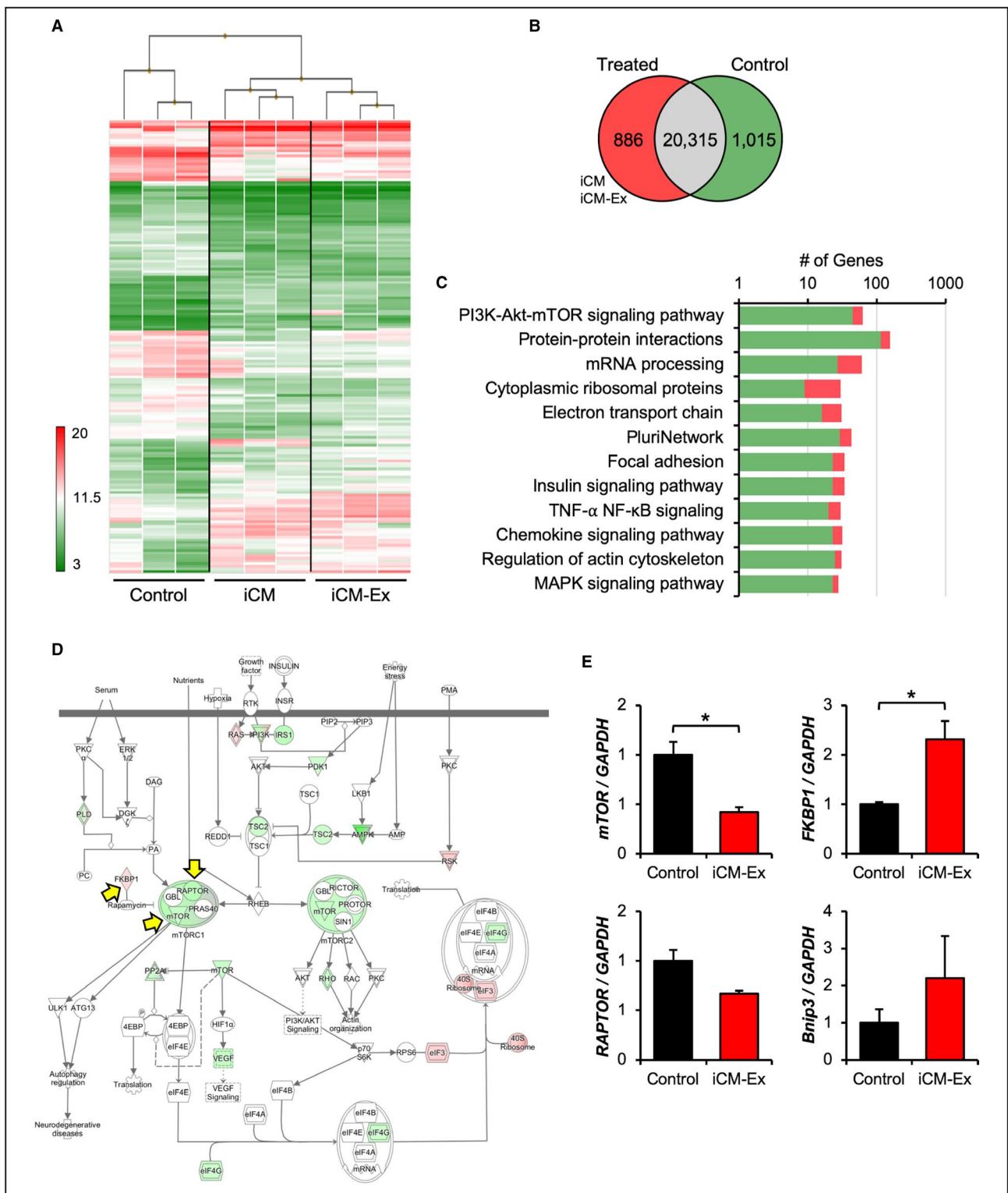


Figure 5. Transcriptomic profiles and mTOR signaling in iCM-Ex PIR.

A, Heat map and hierarchical clustering of transcriptome microarray data. PIR tissue was harvested from saline control (n=3), iCM (n=3), and iCM-Ex (n=3) mice 4 weeks post-MI. RNA was isolated and analyzed by transcriptome microarray. **B**, 1091 differentially expressed genes in treated (iCM, iCM-Ex) mice vs saline control ($P < 0.05$, FDR=0.10). 886 genes were upregulated (>2-fold change), and 1015 genes were downregulated (<2-fold change). **C**, Pathway analysis of differentially expressed genes. **D**, mTOR signaling pathway annotated with differentially expressed genes. **E**, qRT-PCR of PIR tissue from saline control and iCM-Ex mice 4 weeks post-MI to measure expression of genes involved in the mTOR signaling pathway. Data are mean \pm SEM of minimum n=3. * $P < 0.05$. FDR indicates false discovery rate; iCM, induced cardiomyocyte; iCM-Ex, exosomes secreted by iCM; MI, myocardial infarction; PIR, peri-infarct region; and qRT-PCR, quantitative real-time polymerase chain reaction.

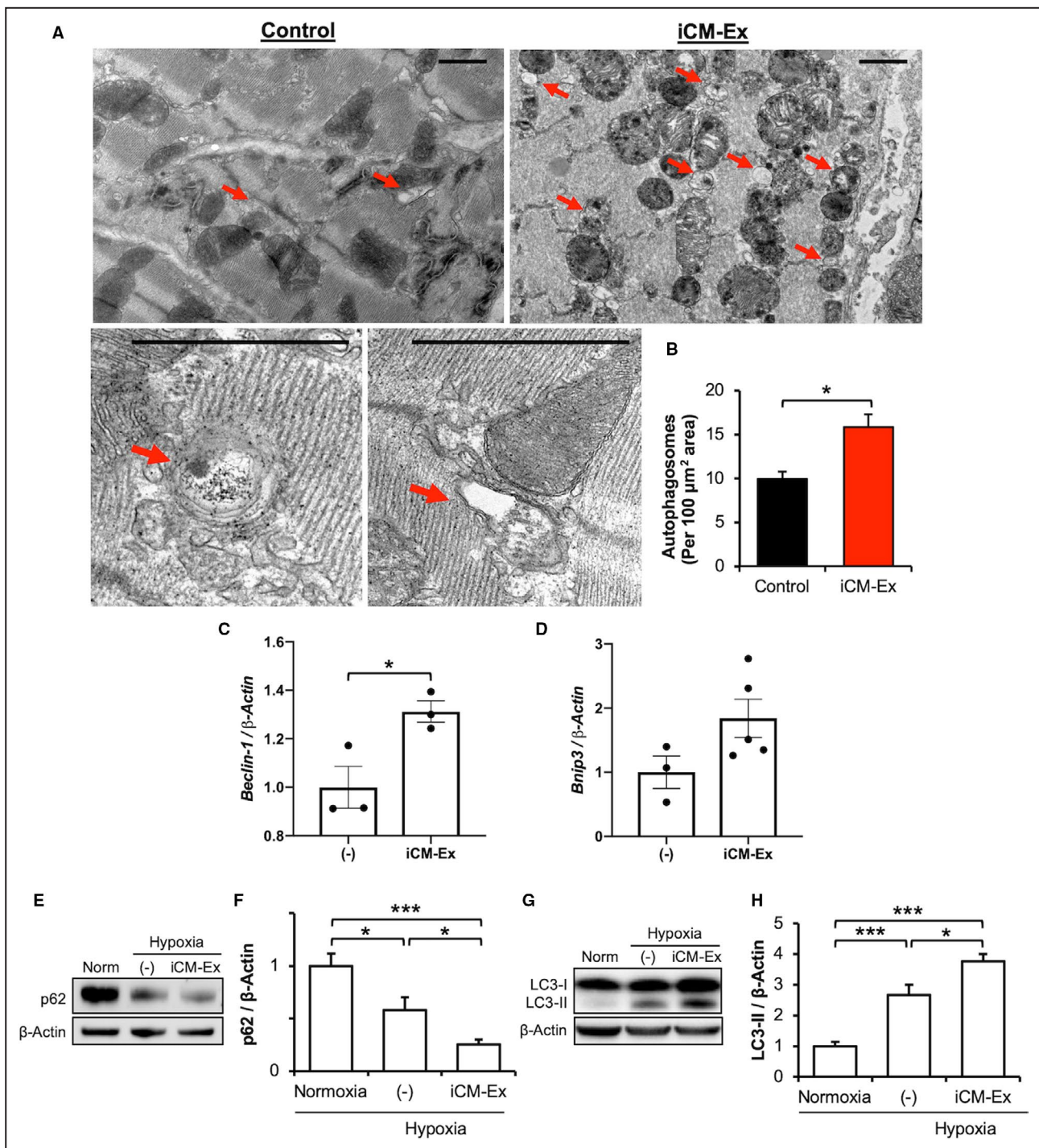


Figure 6. Autophagy is upregulated in hypoxic cells treated with iCM-Ex.

A, Mice were subjected to acute MI, injected with saline control (n=3) vs iCM-Ex (n=5), and euthanized 3 days post-MI. TEM was used to detect autophagosomes in the PIR (red arrows). Scale bar=1 μm. **B**, Quantification of autophagosomes per area. **C**, *Beclin-1* and **D** *Bnip3* gene expression of iCMs exposed to hypoxia and untreated (-) or treated with iCM-Ex. **F**, p62 was detected by IB in normoxic, hypoxic untreated (-), or hypoxic iCM-Ex-treated iCMs. **G**, Densitometric quantitation of p62 expression. **H**, LC3-II was detected by IB in normoxic, hypoxic untreated (-), or hypoxic iCM-Ex-treated iCMs. **I**, Densitometric quantitation of LC3-II expression. Data are mean±SEM of minimum n=3. * $P<0.05$, *** $P<0.001$. IB indicates immunoblotting; iCM, induced cardiomyocyte; iCM-Ex, exosomes secreted by iCMs; MI, myocardial infarction; PIR, peri-infarct region; TEM, transmission electron microscopy; and (-), untreated control.

membrane potential in hypoxic iCMs (Figure S3): hypoxia (-) 0.46 ± 0.06 versus hypoxia rapamycin 0.92 ± 0.12 , $P<0.05$. We therefore hypothesized that

autophagy may be a major mechanism through which iCM-Ex treatment protects cardiomyocytes from ischemia-induced cell death.

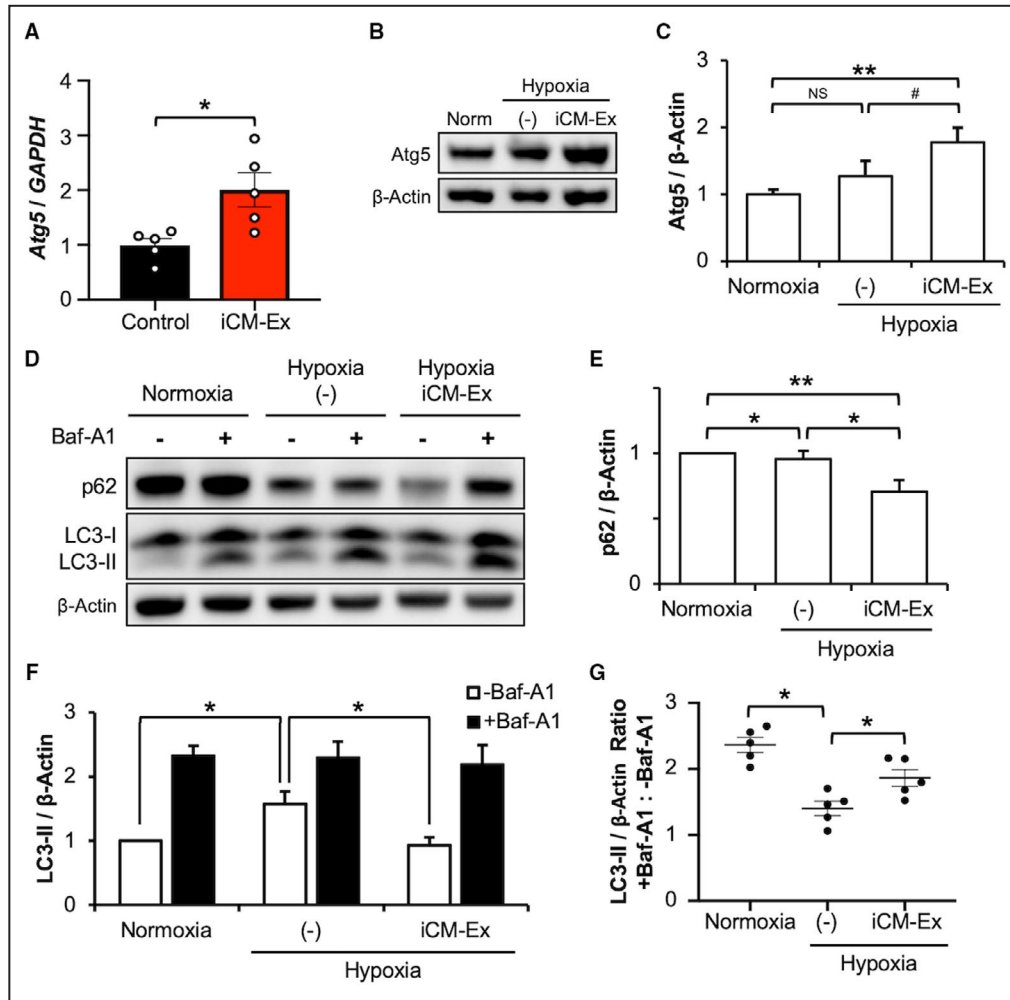


Figure 7. Autophagic flux is enhanced by iCM-Ex.

A, *Atg5* expression in PIR tissue of saline control and iCM-Ex mice measured by qRT-PCR. Samples harvested 4 weeks post-MI. **B**, *Atg5* was detected by IB in normoxic, hypoxic untreated (-), or hypoxic iCM-Ex-treated iCMs. **C**, Densitometric quantitation of *Atg5* expression. **D**, p62 and LC3-II was detected by IB. Groups were treated with 100 nmol/L Bafilomycin A1 4 hours before lysis. **E**, Densitometric quantitation of p62 expression. **F**, Densitometric quantitation of LC3-II expression. **G**, Ratios of LC3-II expression in groups treated with Bafilomycin A1 and untreated. Data are mean \pm SEM of minimum n=3. * P <0.05, ** P <0.01. Baf indicates Bafilomycin; IB, immunoblotting; iCM, induced cardiomyocyte; iCM-Ex, exosomes secreted by iCMs; MI, myocardial infarction; Norm, normal; PIR, peri-infarct region; qRT-PCR, quantitative real-time polymerase chain reaction; and (-), untreated control.

To detect the differences in autophagy in vivo, we performed transmission electron microscopy of the PIR 3 days post-MI (Figure 6A). There were significantly more autophagosomes per unit area in iCM-Ex mice (control 9.9 \pm 0.9 versus iCM-Ex 15.8 \pm 1.5, P <0.05) (Figure 6B). In vitro, we found that iCM-Ex treatment modulates pro-autophagy genes *Beclin-1* and *Bnip3* in hypoxic iCMs, providing further evidence of increased autophagy activation (*Beclin-1* (-) 1.0 \pm 0.9 versus iCM-Ex 1.3 \pm 0.04, P <0.5) (Figure 6C and 6D; Table S4L-K).

We confirmed these findings through examination of well-established protein markers of autophagy. We observed that p62 selectively binds and delivers ubiquitinated proteins to the autophagosome for

degradation. On activation of autophagy, cytoplasmic LC-I protein is cleaved into LC3-II and inserted into the mature autophagosome membrane. Decreases in p62 and increases in LC3-II expression are correlated with increased numbers of autophagosomes. Hypoxia significantly reduced p62 expression (normoxia 1.00 \pm 0.07 versus hypoxia (-) 0.57 \pm 0.07, P <0.05) and increased LC3-II expression (normoxia 1.00 \pm 0.15 versus hypoxia (-) 2.66 \pm 0.33, P <0.001). iCM-Ex treatment further reduced p62 (normoxia versus iCM-Ex 0.25 \pm 0.02, P <0.001; hypoxia versus hypoxia iCM-Ex, P <0.05) and increased LC3-II expression (control versus iCM-Ex 3.76 \pm 0.23, P <0.001; hypoxia (-) versus hypoxia iCM-Ex, P <0.05) (Figure 6F through 6I (-); Table

S3H-L). Therefore, significantly greater quantities of autophagosomes may be found in hypoxic cardiomyocytes treated with iCM-Ex.

Overexpression of autophagy markers can be reflective of a block in autophagosome degradation (ie, reduced autophagic flux) or enhanced autophagosome production matched with ongoing clearance via lysosomal fusion (ie, enhanced autophagic flux). We found upregulation of pro-autophagy gene *Atg5* in the PIR of iCM-Ex mice 4 weeks post-MI, suggesting prolonged autophagy activation (control 1.00 ± 0.12 versus iCM-Ex 2.0 ± 0.3 , $P < 0.05$) (Table S4E, H). Autophagosome accumulation without clearance is associated with cytotoxicity²⁴ and cardiomyocyte death.²⁵ We therefore sought to determine if autophagosomes continued to accumulate or were degraded in hypoxic cardiomyocytes treated with iCM-Ex.

Researchers have reported that hypoxia-ischemia induces autophagic flux in vitro in a time-dependent manner, with a peak between 12 and 24 hours.^{26,27} To allow for autophagosome-lysosome fusion, we extended our hypoxia duration to 18 hours and reduced hypoxic severity to 1% O₂, as prolonged exposure to 0% O₂ resulted in near-total cell death (data not shown). Under these conditions, we found significant overexpression of *Atg5* (normoxia 1.00 ± 0.04 versus iCM-Ex 0.57 ± 0.23) (Figure 7B and 7C) and downregulation of p62 following iCM-Ex treatment (normoxia versus hypoxia iCM-Ex 0.82 ± 0.11 , $P < 0.01$; hypoxia (-) versus hypoxia iCM-Ex, $P < 0.05$) (Figure 7D and 7E; Table S3H, J-M), again demonstrating increased autophagy activation. Interestingly, we found no statistically significant differences between normoxic and hypoxic untreated cardiomyocytes in these markers (Figure 7C through 7E). However, LC3-II was significantly overexpressed in untreated hypoxic cardiomyocytes (normoxia 1.00 versus hypoxia (-) 1.57 ± 0.20 , $P < 0.05$) (Figure 7F; Table S3I-L). We next compared the relative rates of autophagosome clearance or flux, as measured by the ratio of LC3-II expression with and without a lysosome inhibitor, Bafilomycin A1 (Figure 7G). Untreated hypoxic cardiomyocytes had significantly impaired autophagic flux compared with the normoxic control (normoxia 2.33 ± 0.16 versus hypoxia (-) 1.47 ± 0.02 , $P < 0.05$). iCM-Ex-treated groups had significantly reduced LC3-II expression (Figure 7F) (hypoxia (-) versus hypoxia iCM-Ex 0.93 ± 0.11 , $P < 0.05$), but enhanced autophagic flux (hypoxia (-) versus hypoxia iCM-Ex 2.37 ± 0.3 , $P < 0.05$) (Figure 7G). These data suggest that iCM-Ex promotes autophagosome production and restores autophagic flux in hypoxic cardiomyocytes.

DISCUSSION

Exosomes are important messengers of intercellular communication and contain small nucleotides,

proteins, and cytoplasmic content reflective of their parent cell. As such, exosomes have the capacity to mediate the beneficial paracrine effects of stem cell therapy. Previous studies have demonstrated that stem cell-derived exosomes may stimulate cardiac repair following ischemic injury by reducing infarct size (bone marrow-derived mesenchymal stem cell exosomes),²⁸ fibrosis (cardiac progenitor cell exosomes),²⁹ and conferring antiapoptotic signaling to the injured myocardium (human umbilical cord mesenchymal stem cell exosomes).³⁰ Relevant to our studies, several groups have evaluated embryonic stem cell- and iPSC-derived exosomes for repair of myocardial injuries³¹ and have demonstrated improved cardiac function. We previously reported that terminal differentiation of pluripotent stem cells to cardiomyocytes before injection significantly improves the restorative potential of the transplanted cells.⁷ Significant cardiac repair was observed despite poor engraftment, suggesting that putative effects may be largely due to the action of released bioactive molecules. We thus hypothesized that exosomes, a significant constituent of the cell secretome, may mediate iCM-based repair.

Significant Findings

In the present study we examined the therapeutic potential of iCMs and their secreted exosomes (iCM-Ex) for treatment of myocardial infarctions. Our main findings are the following: (1) iCM-Ex enhance cardiomyocyte survival in hypoxia and cardiac function in a murine myocardial infarction model similar to cell transplantation; (2) iCM-Ex confer transcriptional changes to the peri-infarct region, particularly impacting mTOR signaling; and (3) autophagy and autophagic flux are upregulated by iCM-Ex. Our findings indicate that iCM-Ex may be an equally effective bioactive substitute to live cell injections for repair of the ischemic myocardium.

Autophagosome Production and Flux

Previous work from our laboratory demonstrated that transplantation of pluripotent or terminally differentiated stem cells has limited potential to regenerate cardiomyocytes in vivo, but cardiac function can be restored by rescuing the hibernating or injured cardiomyocytes in the sublethal PIR. Autophagy, a conserved degradation process to recycle organelles and protein, is activated during myocardial hypoxia and/or nutrient deprivation.³² The autophagic process is highly dynamic and involves sequestration of cytoplasmic components into an elongating phagophore, maturation of the phagophore into an autophagosome, and autophagosome fusion with a lysosome to degrade and release its contents.³³

The consequences of autophagy upregulation during hypoxia-ischemia stress are complex.

Numerous studies have linked autophagy activation to improvement in cardiac function³⁴ and fibrosis reduction.³⁵ Paradoxically, other groups have demonstrated that overactivation of autophagy in ischemia is pathogenic.^{36,37} The most common methods of measuring autophagic activity include immunoblotting for autophagosome markers. Overexpression, commonly misinterpreted as enhanced autophagy, may instead reflect autophagosome accumulation and a block in degradation.^{33,38} Indeed, there is a growing body of evidence demonstrating that autophagosome clearance is impaired in hypoxia-ischemia and that restoration of this process can promote myocyte survival.^{25,39}

In our study we found that hypoxia-ischemia injury induces a significant increase in autophagosome production in cardiomyocytes. Untreated hypoxic cardiomyocytes demonstrated inconsistent autophagy regulation and impaired flux compared with the normoxic control, whereas iCM-Ex promoted both autophagosome production and clearance. Autophagic flux is necessary to release energy and anabolic building blocks; dysregulation of this process may be detrimental in conditions of stress.⁴⁰ We speculate that increased autophagy may be therapeutic in hypoxia-ischemia injury. Cardioprotective effects may be compromised by inadequate autophagic flux. Increasing both sides of autophagy—formation and degradation—may represent a promising intervention for ischemic cardiomyopathy.

mTOR Signaling

The mTOR signaling pathway is an important regulator of multiple cellular processes, including autophagy, apoptosis, cell growth and metabolism, and protein synthesis.^{41,42} Groups have reported mTOR as a possible target of various stem cell-derived exosomes.^{43,44} Liu and colleagues attribute the cardioprotective role of MSC exosomes to changes in AMPK-mTOR and Akt-mTOR pathways.¹⁵ We demonstrate that iCM-Ex inhibit mTOR signaling in the recipient PIR. This inhibition may be directly affected by exosomal molecules or may be the result of the converging changes to repair the injured heart. Although we found mTOR signaling to be particularly enriched by iCM-Ex treatment, transcriptomic analyses identified other signaling pathways that may contribute to the observed phenotype. Given the complex nature of exosomes and their contents, we postulate that mTOR inhibition and autophagy may not be the only downstream mechanism of iCM-Ex.

Limitations

Although we found the mTOR signaling pathway to be particularly enriched in our iCM-Ex groups, pathway analyses identified other signaling pathways that may

contribute to the phenotype. Finally, although we found a direct correlation between iCM-Ex treatment and mTOR signaling, quantities of autophagosomes, and expression of several autophagy-related genes and LC3B-II protein, further work should be done to elucidate the detailed mechanism behind iCM-Ex modulation of the mTOR signaling pathway and autophagy.

CONCLUSIONS

iCM-Ex transplantation significantly improves cardiac function and myocyte viability and can substitute for parent cell injections. The beneficial effects of iCM-Ex may be partly due to enhanced autophagosome production and flux in hypoxia-ischemia injury. iCM-Ex modulate several signaling pathways in recipient cells, including the mTOR signaling pathway. Future studies of iCM-Ex and their modulation of autophagy may further delineate their potential as a cell-based but cell-free treatment of myocardial infarctions.

ARTICLE INFORMATION

Received August 27, 2019; accepted February 4, 2020.

Affiliations

From the Stanford Cardiovascular Institute (M.R.S., G.I., Y.T., J.-H.J., E.V., P.S., J.C.W., P.C.Y.) and Department of Structural Biology (C.G., D.v.B., S.W.), Stanford University School of Medicine, Stanford, CA; Hard X-ray Department, LCLS (R.G.S.) and Stanford PULSE Institute (R.G.S.), SLAC National Accelerator Laboratory, Menlo Park, CA; Department of Cardiothoracic Surgery, Falk Building, Stanford University Medical Center, Stanford, CA (A.B.G.).

Sources of Funding

This work was supported, in part, by the following awards: 5UM1HL113456-06 (National Institutes of Health), 1 K24 HL130553 (National Institutes of Health), DR2A-05394 (California), and ARRA 1S10RR026780-01 (National Center for Research Resources).

Disclosures

Phillip Yang, MD has received a research grant from the Intervallien Foundation, consults for Terumo Corporation, and co-found of AiCare, Inc.

Supplementary Material

Data S1

Tables S1–S4

Figures S1–S3

Supplemental References 1 and 2

REFERENCES

1. Takahashi K, Tanabe K, Ohnuki M, Narita M, Ichisaka T, Tomoda K, Yamanaka S. Induction of pluripotent stem cells from adult human fibroblasts by defined factors. *Cell*. 2007;131:861–872.
2. Burridge PW, Keller G, Gold JD, Wu JC. Production of de novo cardiomyocytes: human pluripotent stem cell differentiation and direct reprogramming. *Cell Stem Cell*. 2012;10:16–28.
3. Chavakis E, Urbich C, Dimmeler S. Homing and engraftment of progenitor cells: a prerequisite for cell therapy. *J Mol Cell Cardiol*. 2008;45:514–522.
4. Sun Q, Zhang Z, Sun Z. The potential and challenges of using stem cells for cardiovascular repair and regeneration. *Genes Dis*. 2014;1:113–119.
5. Ong SG, Huber BC, Lee WH, Kodo K, Ebert AD, Ma Y, Nguyen PK, Diecke S, Chen WY, Wu JC. Microfluidic single-cell analysis of transplanted human induced pluripotent stem cell-derived cardiomyocytes after acute myocardial infarction. *Circulation*. 2015;132:762–771.

6. Kim PJ, Mahmoudi M, Ge X, Matsuura Y, Toma I, Metzler S, Kooreman NG, Ramunas J, Holbrook C, McConnell MV, et al. Direct evaluation of myocardial viability and stem cell engraftment demonstrates salvage of the injured myocardium. *Circ Res*. 2015;116:e40–e50.
7. Tachibana A, Santoso MR, Mahmoudi M, Shukla P, Wang L, Bennett M, Goldstone AB, Wang M, Fukushi M, Ebert AD, et al. Paracrine effects of the pluripotent stem cell-derived cardiac myocytes salvage the injured myocardium. *Circ Res*. 2017;121:e22–e36.
8. Vestad B, Llorente A, Neurauter A, Phuyal S, Kierulf B, Kierulf P, Skotland T, Sandvig K, Haug KBF, Ovstebo R. Size and concentration analyses of extracellular vesicles by nanoparticle tracking analysis: a variation study. *J Extracell Vesicles*. 2017;6:1344087
9. Barile L, Moccetti T, Marban E, Vassalli G. Roles of exosomes in cardioprotection. *Eur Heart J*. 2017;38:1372–1379.
10. Katsman D, Stackpole EJ, Domin DR, Farber DB. Embryonic stem cell-derived microvesicles induce gene expression changes in Muller cells of the retina. *PLoS One*. 2012;7:e50417.
11. Jung JH, Fu X, Yang PC. Exosomes generated from iPSC-derivatives: new direction for stem cell therapy in human heart diseases. *Circ Res*. 2017;120:407–417.
12. Kishore R, Khan M. More than tiny sacks: stem cell exosomes as cell-free modality for cardiac repair. *Circ Res*. 2016;118:330–343.
13. Mizushima N, Komatsu M. Autophagy: renovation of cells and tissues. *Cell*. 2011;147:728–741.
14. Eskelinen EL, Saftig P. Autophagy: a lysosomal degradation pathway with a central role in health and disease. *Biochim Biophys Acta*. 2009;1793:664–673.
15. Liu L, Jin X, Hu CF, Li R, Zhou Z, Shen CX. Exosomes derived from mesenchymal stem cells rescue myocardial ischaemia/reperfusion injury by inducing cardiomyocyte autophagy via AMPK and Akt pathways. *Cell Physiol Biochem*. 2017;43:52–68.
16. Chen L, Wang Y, Pan Y, Zhang L, Shen C, Qin G, Ashraf M, Weintraub N, Ma G, Tang Y. Cardiac progenitor-derived exosomes protect ischemic myocardium from acute ischemia/reperfusion injury. *Biochem Biophys Res Commun*. 2013;431:566–571.
17. Weng Y, Sui Z, Shan Y, Hu Y, Chen Y, Zhang L, Zhang Y. Effective isolation of exosomes with polyethylene glycol from cell culture supernatant for in-depth proteome profiling. *Analyst*. 2016;141:4640–4646.
18. Trajkovic K, Hsu C, Chiantia S, Rajendran L, Wenzel D, Wieland F, Schwille P, Brugger B, Simons M. Ceramide triggers budding of exosome vesicles into multivesicular endosomes. *Science*. 2008;319:1244–1247.
19. Ibrahim AG, Cheng K, Marban E. Exosomes as critical agents of cardiac regeneration triggered by cell therapy. *Stem Cell Rep*. 2014;2:606–619.
20. Kosaka N, Iguchi H, Hagiwara K, Yoshioka Y, Takeshita F, Ochiya T. Neutral sphingomyelinase 2 (nSMase2)-dependent exosomal transfer of angiogenic microRNAs regulate cancer cell metastasis. *J Biol Chem*. 2013;288:10849–10859.
21. Mittelbrunn M, Gutierrez-Vazquez C, Villarroya-Beltri C, Gonzalez S, Sanchez-Cabo F, Gonzalez MA, Bernad A, Sanchez-Madrid F. Unidirectional transfer of microRNA-loaded exosomes from T cells to antigen-presenting cells. *Nat Commun*. 2011;2:282.
22. Reers M, Smiley ST, Mottola-Hartshorn C, Chen A, Lin M, Chen LB. Mitochondrial membrane potential monitored by jc-1 dye. *Methods Enzymol*. 1995;260:406–417.
23. Wang X, Gu H, Qin D, Yang L, Huang W, Essandoh K, Wang Y, Caldwell CC, Peng T, Zingarelli B, Fan GC. Exosomal MIR-223 contributes to mesenchymal stem cell-elicited cardioprotection in polymicrobial sepsis. *Sci Rep*. 2015;5:13721.
24. Button RW, Roberts SL, Willis TL, Hanemann CO, Luo S. Accumulation of autophagosomes confers cytotoxicity. *J Biol Chem*. 2017;292:13599–13614.
25. Ma X, Liu H, Foyil SR, Godar RJ, Weinheimer CJ, Hill JA, Diwan A. Impaired autophagosome clearance contributes to cardiomyocyte death in ischemia/reperfusion injury. *Circulation*. 2012;125:3170–3181.
26. Zou J, Liu Y, Li B, Zheng Z, Ke X, Hao Y, Li X, Li X, Liu F, Zhang Z. Autophagy attenuates endothelial-to-mesenchymal transition by promoting snail degradation in human cardiac microvascular endothelial cells. *Biosci Rep*. 2017;37. DOI: 10.1042/BSR20171049.
27. Hu Z, Cai HY, Luo YY, Xiao JM, Li L, Guo T. Effect of varying hypoxia reoxygenation times on autophagy of cardiomyocytes. *Acta Cir Bras*. 2018;33:223–230.
28. Lai RC, Arslan F, Lee MM, Sze NS, Choo A, Chen TS, Salto-Tellez M, Timmers L, Lee CN, El Oakley RM, Pasterkamp G, de Kleijn DP, Lim SK. Exosome secreted by MSC reduces myocardial ischemia/reperfusion injury. *Stem Cell Res*. 2010;4:214–222.
29. Maring JA, Beez CM, Falk V, Seifert M, Stamm C. Myocardial regeneration via progenitor cell-derived exosomes. *Stem Cells Int*. 2017;2017:7849851.
30. Zhao Y, Sun X, Cao W, Ma J, Sun L, Qian H, Zhu W, Xu W. Exosomes derived from human umbilical cord mesenchymal stem cells relieve acute myocardial ischemic injury. *Stem Cells Int*. 2015;2015:761643.
31. Khan M, Nickoloff E, Abramova T, Johnson J, Verma SK, Krishnamurthy P, Mackie AR, Vaughan E, Garikipati VN, Benedict C, et al. Embryonic stem cell-derived exosomes promote endogenous repair mechanisms and enhance cardiac function following myocardial infarction. *Circ Res*. 2015;117:52–64.
32. Mazure NM, Pouyssegur J. Hypoxia-induced autophagy: cell death or cell survival? *Curr Opin Cell Biol*. 2010;22:177–180.
33. Klionsky DJ, Abdalla FC, Abeliovich H, Abraham RT, Acevedo-Arozena A, Adeli K, Agholme L, Agnello M, Agostinis P, Aguirre-Ghiso JA, et al. Guidelines for the use and interpretation of assays for monitoring autophagy. *Autophagy*. 2012;8:445–544.
34. Sciarretta S, Volpe M, Sadoshima J. NOX4 regulates autophagy during energy deprivation. *Autophagy*. 2014;10:699–701.
35. Wang L, Yuan D, Zheng J, Wu X, Wang J, Liu X, He Y, Zhang C, Liu C, Wang T, et al. Chikusetsu saponin IVa attenuates isoprenaline-induced myocardial fibrosis in mice through activation autophagy mediated by AMPK/mTOR/ULK1 signaling. *Phytomedicine*. 2018;58:152764.
36. Jia Z, Lin L, Huang S, Zhu Z, Huang W, Huang Z. Inhibition of autophagy by berberine enhances the survival of H9C2 myocytes following hypoxia. *Mol Med Rep*. 2017;16:1677–1684.
37. Wang Y, Wang Q, Zhang L, Ke Z, Zhao Y, Wang D, Chen H, Jiang X, Gu M, Fan S, et al. Coptisine protects cardiomyocyte against hypoxia/reoxygenation-induced damage via inhibition of autophagy. *Biochem Biophys Res Commun*. 2017;490:231–238.
38. Mizushima N, Yoshimori T. How to interpret LC3 immunoblotting. *Autophagy*. 2007;3:542–545.
39. Wang ZG, Li H, Huang Y, Li R, Wang XF, Yu LX, Guang XQ, Li L, Zhang HY, Zhao YZ, et al. Nerve growth factor-induced Akt/mTOR activation protects the ischemic heart via restoring autophagic flux and attenuating ubiquitinated protein accumulation. *Oncotarget*. 2017;8:5400–5413.
40. Lavandro S, Troncoso R, Rothermel BA, Martinet W, Sadoshima J, Hill JA. Cardiovascular autophagy: concepts, controversies, and perspectives. *Autophagy*. 2013;9:1455–1466.
41. Buss SJ, Muenz S, Riffel JH, Malekar P, Hagenmueller M, Weiss CS, Bea F, Bekeredjian R, Schinke-Braun M, Izumo S, et al. Beneficial effects of mammalian target of rapamycin inhibition on left ventricular remodeling after myocardial infarction. *J Am Coll Cardiol*. 2009;54:2435–2446.
42. Sciarretta S, Zhai P, Shao D, Maejima Y, Robbins J, Volpe M, Condorelli G, Sadoshima J. Rheb is a critical regulator of autophagy during myocardial ischemia: pathophysiological implications in obesity and metabolic syndrome. *Circulation*. 2012;125:1134–1146.
43. Liu H, Sun X, Gong X, Wang G. Human umbilical cord mesenchymal stem cells derived exosomes exert antiapoptosis effect via activating PI3K/Akt/mTOR pathway on H9C2 cells. *J Cell Biochem*. 2019;120:14455–14464.
44. Liu H, Sun X, Gong X, Wang G. Human umbilical cord mesenchymal stem cells derived exosomes exert antiapoptosis effect via activating PI3K/Akt/mTOR pathway on H9C2 cells. *J Cell Biochem*. 2019;120:14455–14464.

SUPPLEMENTAL MATERIAL

Data S1.

SUPPLEMENTAL MATERIALS AND METHODS

Preparation of human amniotic membrane-derived mesenchymal stem cells (hAMSCs).

Placenta was donated by families after childbirth at Stanford Department of Obstetrics and Gynecology. Amniotic membrane was isolated, digested, and cultured as previously described¹.

Preparation of mesenchymal stem cell-derived induced pluripotent stem cells (iPSCs).

The monoclonal iPSCs lines were generated by transfection of hAMSCs with non-integrating Sendai virus (Thermo Fisher Scientific Inc., MA), which include *OCT3/4*, *SOX2*, *KLF4*, *L-MYC*, *LIN-28*, short-hairpin RNA for P53 and EBNA1 in chemically defined media. Reprogrammed hAMSCs were transferred onto mouse embryonic fibroblast feeder cells (Cat. A24903, Thermo Fisher Scientific) on 0.1% gelatin-coated plates at day 3 after transfection and cultured in Essential 8 pluripotent stem cell medium (E-8 media, Life Technologies, CA). At day 20 after transfection, nascent iPSC colonies were picked and cultured independently on matrigel-coated plates in E-8 medium. Pluripotency was confirmed through qPCR gene expression analysis of the pluripotency genes *Nanog*, *Oct3/4* and *Sox2* (data not shown).

Preparation and purification of iPSC-derived cardiomyocytes (iCMs).

iPSC monoclonal lines were differentiated into iCMs under chemically defined conditions using small molecules as previously described². 85% confluent iPSCs were incubated with CHIR (6 μ M, D0-2) and then with C59 (2 μ M, D3-5) in basal iCM differentiation medium (Gibco® RPMI 1640 medium, GlutaMAX™ Supplement, Thermo Fisher Scientific) with B-27 Supplement Minus Insulin (Thermo Fisher). On day 6, the medium was replaced with iCM maintenance media (Gibco® RPMI 1640 medium, GlutaMAX™ Supplement, Thermo Fisher Scientific) with B-27 Supplement. Upon spontaneous contractility (days 12-16), cells were replated to new matrigel-coated plates and glucose-free iCM maintenance media for 48 hours for purification.

Nanoparticle tracking analysis (NTA)

Exosome size and quantity were characterized by NTA with a NanoSight LM20 (NanoSight, UK). Samples were loaded into the sample chamber with sterile syringes and imaged using a 640-nm laser. Three measurements of the same sample were performed at room temperature (continuously monitored and manually entered). Particle size and velocity in the fixed chamber was used in a proprietary software, NTA 3.1 (NanoSight), to determine the mean size and standard deviation (SD) values of the particles. To verify that the concentration readings were representative, samples were measured in three serial measurements and averaged per the software protocol. Furthermore, a second set of 3 measurements were done at half or double the concentration, depending on the signal-to-noise from the initial triplicate run. The measured concentrations would be compared. Per protocol, concentrations within 20% of each other were indicative of accurate concentration readings.

Patch clamp analysis

iCMs at days 15-20 were dissociated using TrypLE for 10 min, filtered through a 100 μ M cell strainer (BD Biosciences, CA), counted with a Countess Cell Counter, plated as single cells (1×10^5 cells per well of a 24-well plate) on 8 mm no. 1 glass cover slips (Warner Instruments, CT) coated with Synthemax II-SC (625 ng/cm²) in CDM3 supplemented with 2 μ M thiazovivin and allowed to attach for 72 hr, changing the medium every other day. Cells were then subjected to whole-cell patch clamp at 36-37°C, using an EPC-10 patch-clamp amplifier (HEKA, Germany) attached to a RC-26C recording chamber (Warner Instruments) and mounted onto the stage of an inverted microscope (Nikon, Japan). Sharp microelectrodes were fabricated from standard wall borosilicate glass capillary tubes (BF 100-50-10, Sutter Instruments) using a P-97 Sutter micropipette puller to generate electrodes with tip resistances between 50 M Ω and 70 M Ω when backfilled with 3 M KCl. Cell cultures were perfused with warm (35-37°C) Tyrode's solution consisting of 135 mM NaCl, 5.4 mM KCl, 1.8 mM CaCl₂, 1.0 mM MgCl₂, 0.33 mM

NaH₂PO₄, 5 mM HEPES and 5 mM glucose; pH was adjusted to 7.4 with NaOH. Membrane potential measurements were made using the current clamp mode of the Multiclamp 700B amplifier after electrode potential offset and capacitance were neutralized. Data were acquired using PatchMaster software (HEKA) and digitized at 1.0 kHz. The following are the criteria used for classifying observed action potentials (APs) into ventricular-, atrial- and nodal-like human iPSC-derived cardiomyocytes. For ventricular-like, the criteria were a negative maximum diastolic membrane potential (< -50 mV), a rapid AP upstroke, a long plateau phase, AP amplitude > 90 mV and AP duration at 90% repolarization/AP duration at 50% repolarization (APD₉₀/APD₅₀) < 1.4 . For atrial-like, the criteria were an absence of a prominent plateau phase, a negative diastolic membrane potential (< -50 mV) and APD₉₀/APD₅₀ > 1.7 . For Nodal-like, the criteria were a more positive MDP, a slower AP upstroke, a prominent phase 4 depolarization and APD₉₀/APD₅₀ between 1.4 and 1.7.

Immunogold labeling and transmission electron microscopy (TEM) of the exosomes

Approximately 10×10^9 iCM-Ex (as quantified by NTA) were incubated with mouse anti-CD9 antibody overnight at 4°C. Samples were diluted 1:10 in PBS and incubated with 1.4-nm nanogold-conjugated secondary anti-mouse antibody (Nanoprobes, NY) for one hour, followed by crosslinking with 1% glutaraldehyde for 15 minutes, both at room temperatures. Sample volumes were brought to 500 μ L then filtered through Amicon Ultra 0.5 mL centrifugal filters, MWCO 100 kDA (Millipore Sigma, MO) for buffer exchange according to the manufacturer's recommendations. TEM grids (ultra-thin carbon film supported by Lacey carbon grid 300 mesh, Ted Pella, CA) were glow-discharged (PELCO easiglow) (Ted Pella), applying a current of 35 mA for 60 s. After immunogold labeling and chemical cross-linking, 3 μ l of purified exosome samples were applied to the glow-discharged TEM grid. The sample was incubated on the grid for 60 s for absorption on the carbon, excess liquid was blotted (Whatman filter paper No. 1), followed by staining with a 1% phosphotungstic acid solution for 60 seconds, finally blotted and

dried. The negatively stained sample was mounted on a room-temperature side-entry holder and loaded into a Tecnai F20 TEM (FEI, OR) equipped with a K2 detector (Gatan, CA). The microscope was operated in low gain mode and images were acquired with a nominal magnification of 25,000 \times (corresponding to a pixel size of 1.52 Å / pixel) for a total of 8 seconds (200 ms per frame) with a total dose of 150 electrons / Å². Beam induced motion and stage drift was corrected by whole frame alignments using the MotionCor software tool, bandpass filtered (10 and 200 Å) for visualization purposes and finally analyzed in ImageJ 1.49v (Wayne Rasband, NIH, MA).

Exosome miRNA Isolation

Total RNA was isolated from iCM-Ex using Total Exosome RNA and Protein Isolation Kit (Thermo Fisher Scientific) or from iCMs using miRNeasy Mini Kit (Qiagen, Germany). miRNA array was performed using Affymetrix® FlashTag™ Biotin HSR RNA Labeling Kits (Thermo Fisher Scientific), according to manufacturer's recommendations. Bioinformatics and pathway analyses were performed using Affymetrix® Expression Console (Thermo Fisher Scientific) and Transcriptome Analysis Console (Thermo Fisher Scientific), and Ingenuity Pathway Analysis (IPA, Qiagen).

Murine acute myocardial injury (MI) model

Animal care and interventions were done in accordance with the Laboratory Animal Welfare Act and Stanford University Administrative Panel on Laboratory Animal Care. All animals received humane care and treatment in accordance with the "Guide for the Care and Use of Laboratory Animals" (www.nap.edu/catalog/5140.html). Immunosuppressed female 80-100 day-old SCID-beige female mice (Charles River Laboratories, MA) were anesthetized in an isoflurane inhalational chamber and endotracheally intubated with a 20-gauge angiocatheter (Ethicon Endo-Surgery, NJ). Ventilation was maintained with a Harvard rodent ventilator (Harvard Apparatus, MA). Acute MI was created by ligation of the mid left anterior descending coronary artery

(LAD) through a left thoracotomy. A blinded surgeon injected 60 μ l of iCM-exosomes (400×10^8) or iCMs (500,000) suspended in a 1:1 mixture of PBS and Matrigel into the myocardium at the border peri-infarct region (PIR): iCM-Ex (n=8), 2) iCMs (n=6), control (n=11).

Magnetic resonance imaging (MRI)

Cardiac MRI (Signa 3T HDx) (GE Healthcare, WI) was performed using a dedicated mouse coil (Rapid MR International, OH). Mice were imaged at weeks 2 and 4 after LAD ligation. Mice were anesthetized with 1-2% isoflurane at 2L/min oxygen and placed in the supine position. Electrocardiographic gating was obtained with two subcutaneous precordial leads and body temperature was monitored with a rectal probe during the entire scan (SA Instruments, NY). Left ventricular function was evaluated with electrocardiographically triggered Fast Spoiled Gradient-Recalled (FSPGR) sequence (TR 24ms, TE 10ms, FA 45, field of view (FOV) 6 cm², matrix 256 \times 256, slice gap 0mm, slice thickness 1 mm, NEX 4, 2 excitations, and 20 cardiac phases). Manganese-enhanced MRI (MEMRI) was performed using fast gradient echo-inversion recovery (FGRE-IR) sequence (TR 13ms, TE 6ms, FA 30°, FOV 4cm², matrix 256 \times 256, slice gap 0mm, slice thickness 1mm, 2R-R acquisition, TI 300-500ms, and NEX 2) after 40 minutes with intraperitoneal (IP) injection of 0.7cc/kg of SeeMore (Eagle Vision Pharmaceutical, PA) prior to MEMRI acquisition 8, 9. The Mn²⁺-based contrast agent in MEMRI is taken up by L-type calcium channel to generate T1-shortening and positive signal, conferring high specificity to the viable myocardium. The images were analyzed offline using Osirix (Pixmeo, Switzerland) with manual contouring. Tracings of MEMRI was generated for each shortaxis slice and integrated to determine viable myocardial volumes in murine hearts. Percent MEMRI viable myocardial volume = (MEMRI enhancement volume \times 100)/total left ventricular (LV) mass volume.

EdU Staining for Endogenous Proliferation

Mice were injected intraperitoneally with 0.1 mg EdU (Thermo Fisher Scientific) per gram body weight every 24 hours for 2 days prior to sacrifice, heart explantation, and preservation in OCT. 5 μ m sections of the mid-ventricle were stained with Click-iT EdU Staining Kit (Thermo Fisher Scientific), cardiac troponin I (Thermo Fisher Scientific), and Hoechst 33342 per the manufacturers' recommendations. TNNI3 expression was used to locate the PIR. Images were acquired using a LSM 880 inverted confocal microscope (Zeiss, Germany). Number of cells expressing EdU-TNNI3 normalized to number of nuclei (representative of cell number).

***Ex vivo* mouse transcriptome analysis**

Mice were sacrificed 4 weeks post-MI. The PIR was isolated, homogenized, and RNA was isolated with miRNeasy® Mini Kit (Qiagen) according to manufacturers' recommendations. mRNA was arrayed using Clariom™ S Assays (Thermo Fisher) according to the manufacturers' recommendations. Bioinformatics and pathway analyses were performed using Affymetrix® Expression Console (Thermo Fisher Scientific) and Transcriptome Analysis Console (Thermo Fisher Scientific), and Ingenuity Pathway Analysis (IPA) (Qiagen). >2-fold differences in expression were considered significant.

***Ex vivo* RT-PCR analysis of the myocardial tissues**

RT-PCR was performed to verify significant gene expression as determined by the mouse transcriptome arrays. Total RNA, isolated using miRNeasy® Mini Kit (Qiagen) and verified with NanoDrop 2000 (Thermo Fisher Scientific), was reverse-transcribed with Applied Biosystems™ High-Capacity cDNA Reverse Transcription Kit (Thermo Fisher Scientific). Relative gene expression was measured by Applied Biosystems™ StepOne Plus™ Real-Time PCR System (Thermo Fisher Scientific). GAPDH was used as an internal housekeeping gene. All reagents and instruments were used according to manufacturers' recommendations. Primer sequences can be found in Table S1.

Fibrosis Quantification

10 µm sections of the mid-ventricle were stained with Masson's Trichrome Stain Kit (Polysciences Inc., PA) per the manufacturer's recommendations. Images were acquired using a BZ-X710 microscope (Keyence, Japan). Fibrotic area (dark blue-stained tissue) in the left ventricle was normalized to the entire cross-sectional area.

Terminal deoxynucleotide Transferase dUTP Nick-End Labeling (TUNEL)

5 µm sections of the mid-ventricle were stained with Click-iT TUNEL Staining Kit (Thermo Fisher Scientific), cardiac troponin I (Thermo Fisher Scientific), and Hoechst 33342 per the manufacturers' recommendations. Images were acquired using a LSM 880 inverted confocal microscope (Zeiss). Number of cells co-expressing TUNEL and TNNI3 was normalized to number of nuclei (representative of cell number).

Inhibition of Exosome Secretion

Manumycin A (Millipore Sigma) was reconstituted in DMSO. To fully inhibit exosome secretion, cells were pre-treated with 10 µM MA for 24 hours prior to assays.

Mitochondrial membrane integrity measurement of hypoxic cardiomyocytes

At the end of hypoxia exposure, JC-1 Mitochondrial Membrane Potential Probe (Cayman Chemicals, MI) was added to sample medium at concentration of 100 µL per 1 mL culture medium and incubated for 30 min at 37°C. Images were acquired using an BZ-X710 microscope (Keyence) and analyzed with ImageJ (NIH).

Transmission Electron Microscopy

On day 3 post-MI, mice were sacrificed and the hearts were perfused with Karnovsky's fixative (2% glutaraldehyde, 4% paraformaldehyde, in 0.1M sodium cacodylate pH 7.4). Tissue in the PIR were cut into approximately 1 mm² blocks and returned to fixative solution for 1 hour. The fix was replaced with cold/aqueous 1% osmium tetroxide and were then allowed to warm to room temperature (RT) for 2 hours rotating in a hood, washed 3X with ultrafiltered water, then

en bloc stained in 1% uranyl acetate at RT for two hours while rotating. Samples were then dehydrated in a series of ethanol (EtOH) washes for 30 minutes each at RT beginning at 50%, 70% ethanol then moved to 4°C overnight. They were placed in cold 95% EtOH and allowed to warm to RT, changed to 100% 2X, then propylene oxide (PO) for 15 min. Samples are infiltrated with EMbed-812 resin (Thermo Fisher Scientific) mixed 1:2, 1:1, and 2:1 with PO for 2 hrs each with leaving samples in 2:1 resin to PO overnight rotating at RT in the hood. The samples are then placed into EMbed-812 for 2 to 4 hours then placed into molds and fresh resin, orientated and placed into 65°C oven overnight. Images were acquired with a JEM1400 120kV Transmission Electron Microscope with a Gatan Orius CCD Camera (JEOL, MA).

Autophagosomes were identified as double-membrane-bound vesicles containing organelle-like structures and quantified as the average of 20 random micrographs per animal.

RT-PCR

iCM RNA was isolated using miRNeasy Mini Kit (Qiagen) and reverse transcribed using High Capacity RNA-to-cDNA Kit (Thermo Fisher Scientific). Equal amounts of cDNA were loaded onto a 96-well plate for RT-PCR using in-house primers and Power SYBR Green PCR Master Mix (Thermo Fisher Scientific). Relative gene expression was measured by Applied Biosystems™ StepOne Plus™ Real-Time PCR System (Thermo Fisher Scientific). β -actin was used as an internal housekeeping gene. A list of primers can be found in Table S3.

SDS-PAGE and Immunoblot

Proteins were separated at 10% SDS-PAGE (Thermo Fisher Scientific) under reducing conditions and electrophoretically transferred onto polyvinylidene difluoride membranes (Biorad), followed by routine immunoblotting (IB). Antibodies can be found in Supplementary Table 3.

Table S1. Qualitative and quantitative criteria for classification of iCMs in three major cardiac cell types.

Nodal-like (N-like):

- Always generated spontaneous APs
- Exhibits a more depolarized MDP
- A prominent phase 4 depolarization
- Slower maximum rate of rise
- Shortest APD
- APD90/APD50: 1.4-1.7

Atrial-like (A-like):

- Triangular AP profile
- Absence of a prominent plateau phase
- A negative MDP (< -50 mV)
- More hyperpolarized MDP/RMP
- A faster rate of rise
- Intermediate APD
- APD90/APD50: > 1.7

Ventricular-like (V-like):

- A negative MDP (< -50 mV),
 - A rapid AP upstroke,
 - A long plateau phase,
 - APA > 90 mV
 - APD90/APD50: < 1.4
-

Table S2. Summary of action potential parameters of iCMs day 15-19 day of differentiation.

iCMs (n=23)	% of cells (n)	Beating rate (bpm)	MDP (mV)	Overshoot (mV)	APA (mV)	APD90 (ms)	APD70 (ms)	APD50 (ms)	V_{max} (V/Sec)
Ventricular-like	65 (15)	42.0 ± 4.3	-53.5 ± 1.0	39.3 ± 0.8	92.8 ± 1.2	342.4 ± 18.7	324.4 ± 17.5	302.1 ± 16.3	19.2 ± 0.9
Atrial-like	26 (06)	40.0 ± 1.1	-52.1 ± 1.6	38.4 ± 2.2	90.5 ± 3.3	259.1 ± 44.0	219.4 ± 37.9	177.4 ± 28.8	18.5 ± 1.7
Nodal-like	09 (02)	68.0 ± 1.9	-40.9 ± 1.2	27.0 ± 1.8	67.9 ± 3.0	236.4 ± 35.6	175.9 ± 47.6	140.6 ± 34.6	5.8 ± 1.8

BPM: Beat Per Minute

MDP: Maximal Diastolic Potential

APA: Action Potential Amplitude

APD₅₀: Action Potential Duration at 50% repolarization

APD₇₀: Action Potential Duration at 70% repolarization

APD₉₀: Action Potential Duration at 90% repolarization

V_{max}: Upstroke Velocity

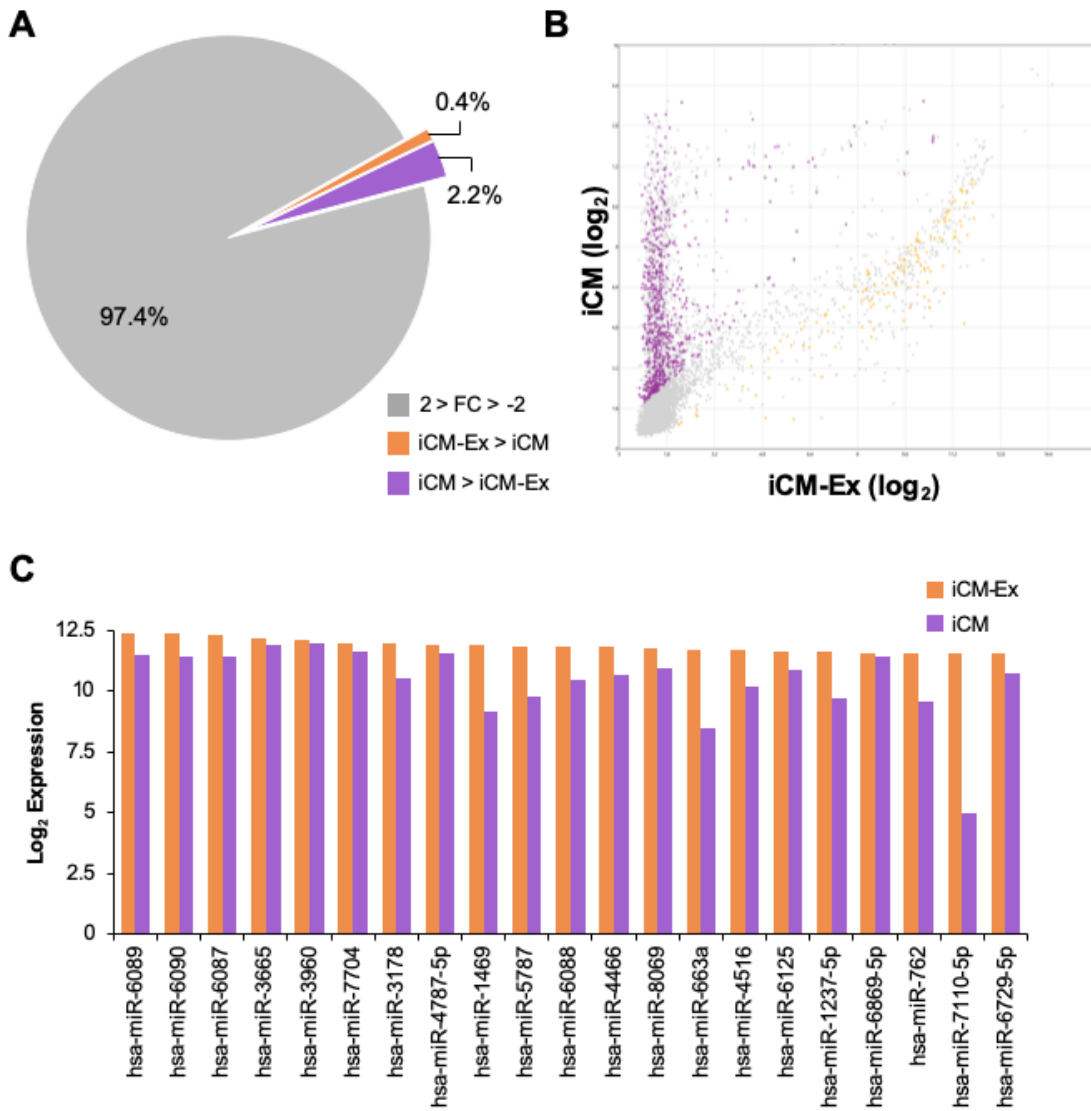
Table S3. Antibody Dilutions and Vendor Information.

Antibody	Dilution	Manufacturer	Catalog No.
A. Mouse anti-Human CD63	1:500	Abcam	Ab8219
B. Donkey anti-Mouse IgG (H+L), Alexa Fluor 700	1:10,000	Thermo Fisher Scientific	A10038
C. Mouse anti-Human CD9	1:500	Thermo Fisher Scientific	10626D
D. Nanogold anti-Mouse Fab' fragment	1:1,000	Nanoprobes	2002
E. Monoclonal Anti- α -Actinin (sarcomeric)	1:600	Millipore Sigma	A7811
F. Hoechst 33342, Trihydrochloride, Trihydrate	2 μ g/mL	Thermo Fisher Scientific	H3570
G. Rabbit anti-Human, -Mouse, -Rat Troponin I	1:200	Thermo Fisher Scientific	701585
H. Rabbit anti-Human, -Mouse, -Rat p62	1:1,000	Cell Signaling Technology	5114
I. Rabbit anti-Human, -Mouse, -Rat LC3B	1:1,000	Cell Signaling Technology	2775
J. Monoclonal Anti- β -Actin	1:5,000	Millipore Sigma	A5441
K. Anti-Rabbit IgG, HRP Conjugate	1:5,000	Promega	W4011
L. Anti-Mouse IgG, HRP Conjugate	1:5,000	R&D	HAF007
M. Rabbit anti-Human, -Mouse, Rat Atg5	1:1,000	Cell Signaling Technology	2630

Table S4. Primer Sequences.

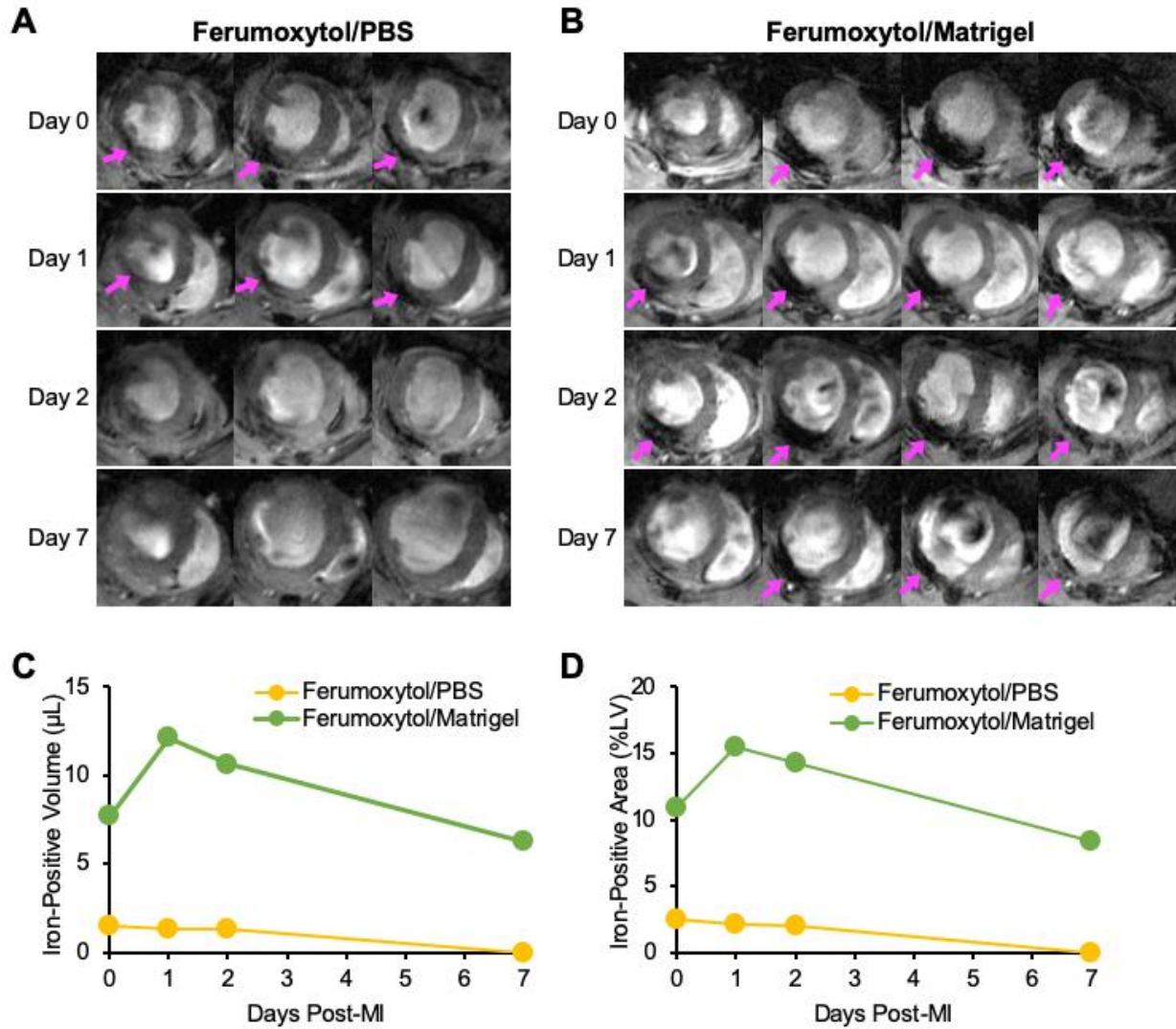
Species	Primer Name	Forward Sequence	Reverse Sequence
	A. <i>BCL-2</i>	AGTTCGGTGGGGTCATGTGTG	CCAGGTATGCACCCAGAGTG
	B. <i>BCL-xL</i>	CACTGTGCGTGGAAAGCGTAG	CGACTGAAGAGTGAGCCCAG
	C. <i>GAPDH</i>	AACTTTGGCATTGTGGAAGG	ACACATTGGGGGTAGGAACA
<i>Mus</i>	D. <i>mTOR</i>	AGAGGTCGGCACTCCACTAT	TGGCCAGGCTTCTGAACAAA
<i>Musculus</i>	E. <i>FKBP1</i>	AAGGGGTAGCCCAGATGAGT	CAGATCCACGTGCAGAGCTAA
	F. <i>RAPTOR</i>	TCTTATGGGACTCGGGGAGG	TGTGGTCTTCACCACATCCG
	G. <i>Bnip3</i>	ACGAACCCCACTTTGCAGTT	CCACCCAAGGTAATGGTGGA
	H. <i>Atg5</i>	GACGTTGGTAACTGACAAAGTGA	GCCATTTTCAGTGGTGTGCCT
	L. <i>β-actin</i>	TCCCTGGAGAAGAGCTACGA	AGCACTGTGTTGGCGTACAG
<i>Homo sapiens</i>	J. <i>Beclin-1</i>	GGGTTGCGGTTTTTCTGGGA	GTGTCTCGCCTTTCTCAACC
	K. <i>BNIP3</i>	AAGGCGTCTGACAACCTCC	GAGCTATGTTGCAAGCTCAGA

Figure S1. miRNA Profiles of iCMs and iCM-Ex.



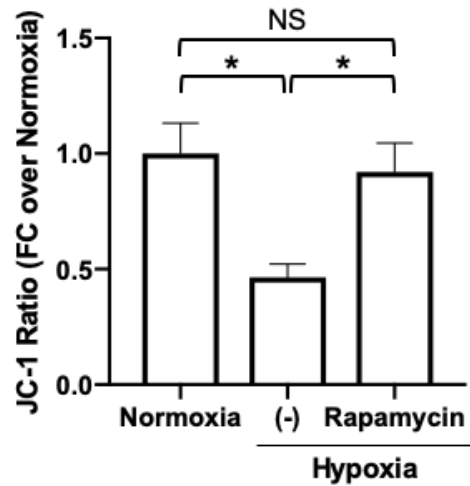
miRNA content of iCM and iCM-Ex were characterized by microarray. (A) The majority of miRNAs (97.4%) were expressed at similar levels (less than 2-fold change (FC)). (B) Relative expression levels of iCM and iCM-Ex miRNAs. (C) Top 20 highly expressed miRNAs in iCM-Ex and their respective expression in iCMs.

Figure S2. Matrigel enhances long-term retention of injected nanoparticles in myocardium.



Mice received acute MI and were injected with Ferumoxytol nanoparticles in the peri-infarct border. Prior to injection, Ferumoxytol was suspended in a solution of Matrigel/PBS or PBS alone. The mouse myocardium was imaged by cardiac MRI for 7 days post-MI. Hypointense signals denoted the presence of Ferumoxytol (pink arrows) in (A) mice injected with Ferumoxytol in PBS alone and (B) mice injected with Ferumoxytol in PBS with Matrigel. Ferumoxytol injected with Matrigel was detectable 7 days post-MI while Ferumoxytol injected with PBS alone failed to be detected by day 2. The hypointense signals generated by Ferumoxytol were quantified and plotted as (C) volume and (D) percentage of LV. Mice treated with Ferumoxytol/Matrigel showed greater iron-positive volume and iron-positive area than mice treated with Ferumoxytol/PBS.

Figure S3. Autophagy preserves mitochondrial membrane potential in hypoxic cardiomyocytes in vivo.



Mitochondrial membrane potential (MMP) was assessed by JC-1 fluorescent assay in three groups: normoxia, hypoxia untreated (-) control, hypoxia + rapamycin (scale bar = 100 μ m). (B) MMP is significantly reduced in hypoxic (-) or MA-treated cells and restored by rapamycin treatment. Data are mean \pm SEM of minimum n=3. *p<0.05.

SUPPLEMENTAL REFERENCES:

1. Ge X, Wang IN, Toma I, Sebastiano V, Liu J, Butte MJ, Reijo Pera RA, Yang PC. Human amniotic mesenchymal stem cell-derived induced pluripotent stem cells may generate a universal source of cardiac cells. *Stem Cells Dev.* 2012;21:2798-2808.
2. Kim PJ, Mahmoudi M, Ge X, Matsuura Y, Toma I, Metzler S, Kooreman NG, Ramunas J, Holbrook C, McConnell MV, Blau H, Harnish P, Rulifson E, Yang PC. Direct evaluation of myocardial viability and stem cell engraftment demonstrates salvage of the injured myocardium. *Circ Res.* 2015;116:e40-50.